https://doi.org/10.5194/egusphere-2026-871
Preprint. Discussion started: 4 March 2026

Post-deposition processes affecting water stable isotope records at Little Dome C, Antarctica: new records from two firn cores and virtual firn core modelling

Emma Samin[1], Amaëlle Landais[1], Elise Fourré[1], Mathieu Casado[1], Adrien Ooms[1], Niels Dutrievoz[1], Cécile Agosta[1], Valérie Masson-Delmotte[1], Thomas Combacal[1], Elsa Gautier[2], Bénédicte Minster[1]

[1]LSCE/IPSL, CEA-CNRS-UVSQ, Université Paris-Saclay, Gif-sur-Yvette, France
[2]Université Grenoble Alpes, CNRS, IRD, Grenoble INP, INRAE, IGE, 38000 Grenoble, France
Correspondence to: Emma Samin (emmasamin.es@gmail.com)

Abstract. The variability of water isotopes in Antarctic ice cores is of major interest for reconstructing past climate through changes in temperature and the hydrological cycle. Archived during the deposition of successive layers of snow, water molecules undergo various processes that can modify the isotopic signal initially imprinted in snowfall during the process of snow densification to ice (i.e. firn). Diffusion is a well-known effect that affects water isotope composition by smoothing the initial climate-related signal. Here, we focus on new water isotopes profiles of two firn cores from Little Dome C (LDC), dated thanks to sulphate concentration measurements, with the aim to identify the physical processes affecting the isotopic signal in the firn at the drilling site for the new Beyond Epica Oldest Ice (BELDC) deep ice core on the East Antarctic Plateau. We use a simple Virtual Firn Core model (VFC) to best fit our $\delta^{18}O$ firn profiles. We conclude that the VFC should include a 8 cm surface mixing layer and that diffusion is overestimated below a depth of 3 meters.

https://doi.org/10.5194/egusphere-2026-871
Preprint. Discussion started: 4 March 2026

1 Introduction

The physico-chemical composition of ice and air bubbles trapped inside preserves highly precise climatic information, making ice cores extremely valuable paleoclimatic archives (Jouzel and Masson-Delmotte, 2010, and references therein). Each layer of snow deposited in polar regions preserves an imprint of the local and global climatic conditions at the time of precipitation. The accumulation rate on the East Antarctic Plateau is one of the lowest on Earth, allowing the preservation of a very long climate history in the ice stratigraphy. In 2004, the end of the drilling of the EPICA Dome C (EDC) deep ice core enabled reconstruction of past Antarctic climate variability over 800,000 years (EPICA Community members, 2004) and records of the glacial and interglacial cycles from Marine Isotopic Stage (MIS) 19 onwards (Jouzel et al., 2007). Recently, the ambition to produce an even older record led to the drilling of the Beyond Epica Oldest Ice (BELDC) deep ice core at Little Dome C (LDC), about 35 km from the previous deep drilling site (Chung et al., 2023), to reach older ice layers. This new core is expected to reveal unprecedented glacial and interglacial cycles and to relate the climate history from more than one million years ago (Barbante and the Beyond EPICA Team, EGU 2025). The BELDC core would provide a unique opportunity to characterize the Mid-Pleistocene Transition, a key period during which the periodicity of glacial/interglacial cycles changed from 41,000 years (early Pleistocene) to 100,000 years (late Pleistocene) (1.2 Ma to ~600 ka, see Berends et al., 2021), and to retrace the temperature and atmospheric composition variability with a high degree of precision.

Among the wide range of climatic properties preserved in ice, water stable isotopes are valuable proxies for continuous past temperature reconstructions as they are sensitive to every phase change along the water cycle. In the 1960s, Dansgaard (1964) and Lorius et al. (1969) demonstrated the empirical relationship between the isotopic composition of precipitation and surface snow, and local surface temperature, with a dependency on moisture transport distance and air mass elevation. This relationship is due to the temperature-dependent distillation of water associated with fractionation between the heavy and light isotopes of oxygen (^{18}O, ^{17}O, ^{16}O) and hydrogen (D, H) that compose the water molecule. Therefore, the atmospheric air mass keeps the imprint of the successive condensation and fractionation events that occur during the moisture transport from the oceanic evaporation area and the precipitation site (Dansgaard, 1964, Craig and Gordon, 1965).

The isotopic signature of water is expressed through the δ notation as (Eq. 1) for oxygen isotopes:

$$\delta^{18}O\ (‰) = \left(\frac{\left(\frac{^{18}O}{^{16}O}\right)_{sample}}{\left(\frac{^{18}O}{^{16}O}\right)_{VSMOW}} - 1\right) * 1000 \quad (Eq.1)$$

VSWOM is the Vienna Standard Mean Ocean Water isotopic standard reference, and is given in ‰.

However, the interpretation of the water isotopic signal is subject to several factors which modify the relationship between the isotopic composition of snow and ice and the atmospheric temperature. Indeed, multiple processes can modify the isotopic signal during and after deposition, post-deposition effects being especially important in areas of low accumulation and long snow surface exposure (Touzeau et al., 2016). First, the isotopic record depends on the temperature when precipitation occurs which leads to a record largely influenced by the precipitation intermittency (Persson et al., 2011, Casado et al., 2018, 2020). Second, the topography of the site and wind blowing can lead to patchy deposition, depending on the surface roughness (Groot Zwaaftink et al., 2013,

https://doi.org/10.5194/egusphere-2026-871
Preprint. Discussion started: 4 March 2026

Libois et al., 2014, Genthon et al., 2016, Picard et al., 2019). This effect is often described as a stratigraphic noise which adds up to the initial climate signal (Fisher et al., 1985, Münch et al., 2016, 2017, Münch and Laepple, 2018, Hirsch et al., 2023). Ritter et al. (2016), Wahl et al. (2022), and Dietrich et al. (2023) also show non-negligible exchanges between surface snow and atmospheric water vapour during summer which has a significant impact on the surface snow isotopic composition (Casado et al., 2021, Ollivier et al., 2025). Finally, molecular diffusion in firn is expected to have the effect of a low-pass filter either fully erasing or reducing the amplitude of the climatic signal and/or noise for high frequencies in the archived signal (Johnsen, 1977, Johnsen et al., 2000, Gkinis et al., 2014, Laepple et al., 2018). Laepple et al. (2018) showed that diffusion can create an apparent wavelength of 20 cm at several very low accumulation sites in Antarctica which does not relate to any climatic signal but to the diffusion associated with stratigraphic noise. Diffusion is often described using the Johnsen et al. (2000) formulation in which diffusion occurs in the water vapor and is limited by the firn tortuosity. Diffusion is then implemented in firn models, characterised by the depth, the accumulation rate and the temperature-dependent diffusion length σ (Gkinis et al., 2014).

As a result, while near-seasonal resolution is achievable in areas with high accumulation rates such as Greenland (Vinther et al., 2010) or coastal and central Antarctica (Morgan, 1985, Masson-Delmotte et al., 2003, Küttel et al., 2012, Jones et al., 2023), the ability to extract meaningful or robust climate signals from firn and ice core records on timescales shorter than multidecadal for the East Antarctic Plateau remains debated (Ekaykin et al., 2002, Pol et al., 2010, Münch et al., 2016, Landais et al., 2017, Casado et al., 2020). Indeed, the comparison of neighbouring snow pits with each other and with surface climate data shows a large variability in isotopic profiles on a short spatial scale which cannot be explained by a direct record of the climatic signal (Laepple et al., 2018, Casado et al., 2018). Because post deposition effects have a stronger effect in low accumulation sites, it is of primary importance to perform surface snow and firn studies to better interpret the isotopic records in deep ice cores.

In this study, we present the first analyses of two shallow cores drilled near the BELDC drilling point. After the presentation of the methods, we present the ICORDA-LDC and Subglacior-LDC age models based on dating sulphate peaks identified as volcanic events, as well as the $\delta^{18}O$ profiles. For a site with very low accumulation rate such as LDC (Gautier et al., 2021), two firn cores are not sufficient to extract an annual climate signal (Casado et al., 2023), so we do not aim to present a climate interpretation of isotopic profiles. Rather, we investigate the physical characteristics, and specifically the frequencies distribution and amplitude, of the $\delta^{18}O$ signal recorded at LDC. To do this, we use a virtual firn core (VFC) model, which simulates the progressive accumulation of snow layers of isotopic composition and widths inferred from the isotopic composition and snowfall rate of each precipitation events extracted from the output of an atmospheric general circulation model (here LMDZ6-iso, Risi et al., 2010, Hourdin et al., 2020). The VFC model also includes description of diffusion and noise. We confront our two firn cores with the results of the VFC model and test adjustments to model parametrizations to best fit the observations at the drilling site of the BELDC core.

2 Methods

In this study, we focus on two shallow cores, Subglacior-LDC (120 m depth long, -75°30.752 S, 122°47.338 E) and ICORDA-LDC (130 m depth long, 75°17.586 S, 122°24.808 E), both drilled around Little Dome C, Antarctica (Fig. 1) in January 2018 and January 2023 respectively. These campaigns aimed to characterise the site around the future deep ice core, by conducting surface process studies to better constrain the climate record in the firn layers.

https://doi.org/10.5194/egusphere-2026-871
Preprint. Discussion started: 4 March 2026

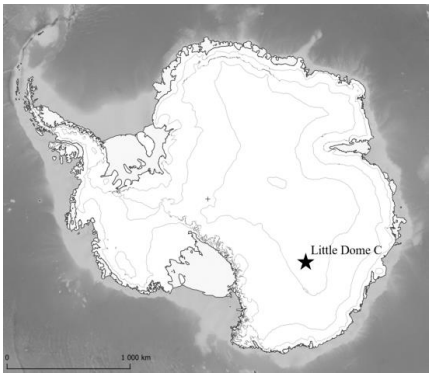

Figure 1 - Location of Little Dome C (LDC), Antarctica

2.1 Firn cores analysis

The Subglacior-LDC firn core was measured at the Laboratoire des Sciences du Climat et de l'Environnement (LSCE) for water isotopes in 2022-2023, and at the Institut des Géosciences de l'Environnement (IGE) for chemistry. The sulphates profile was published by Gautier et al. (2021) and is available online (DOI: https://doi.pangaea.de/10.1594/PANGAEA.932490) over 42 m of firn. Water isotopes were measured over 30 m of the core from discrete samples (2 to 3 cm depth resolution), by laser spectrometry using a ®Picarro L2130-i.

The ICORDA-LDC firn core was measured in March 2024 using a Continuous Flow Analysis (CFA) facility, paired with a ®Picarro L2130-i water vapor analyser for continuous water isotope measurements on one side, and with a fraction collector for off-line ion chromatography analysis on the other side. The upper three meters of the firn core required discrete sampling due to the low structural integrity of the surface layer. For this part, samples of 2.5 cm were cut and melted individually into centrifuge tubes. For the other part of the core (81 m), sticks of 1.00 x 0.03 x 0.03 m were cut and continuously melt and analysed by CFA. The CFA facility of the LSCE is set up on the model of Dallmayr et al. (2016, 2025) and has been described in Petteni et al. (2025). It is characterized by three main units:

(i) The melting system in the cold room to generate a continuous stream of liquid water. The ice sticks are loaded vertically above the melt head, with a mobile encoder on top, recording its position while melting, at a frequency of ~1 Hz. Combined with the stick length, it allows to determine the depth scale for the continuous measurements. The melting rate is approximatively 2.5 ± 0.5 $cm.min^{-1}$. Only the water from the inner part of the stick (18x18 mm) is transferred for analysis, thus eliminating contamination due to handling for the subsequent chemistry analysis. The inner meltwater is sucked up by peristatic pumps out of the cold room to CFA line.

(ii) The isotope measurement unit. A homemade vaporiser at 170°C flushed by a constant flow of dry nitrogen converts the liquid water to vapor, feeding a ®Picarro L2130-i laser spectrometer. Water and nitrogen are set to maintain a humidity level between 18,000 and 22,000 ppm inside the spectrometer cavity, a range for which the humidity dependency of the isotopic measurements has been checked to be negligible.

https://doi.org/10.5194/egusphere-2026-871
Preprint. Discussion started: 4 March 2026

(iii) The fraction collector under a laminar flow hood, protected from external contamination by a parafilm. It collects discrete 3 mL samples in vials protected by parafilm before being capped, and the sampling resolution varies between 0.015 to 0.032 m depending on the core density.

2.2 Isotopes data calibration and resolution

For discrete $\delta^{18}O$ measurements, the analytical uncertainty of the ®Picarro instrument is established at ± 0.20 ‰ (1σ). Calibration and correction were performed using the in-house working standard OC4 ($\delta^{18}O$: -53.93 ± 0.05 ‰), calibrated and corrected against the reference standards EPB9 ($\delta^{18}O$: -7.42 ± 0.05 ‰), Ross7 ($\delta^{18}O$: -18.94 ± 0.05 ‰), and NEEM2 ($\delta^{18}O$: -32.89 ± 0.05 ‰).

For the CFA, the calibration of isotope data was carried out by measuring standards at the beginning and end of the day of continuous analysis. The data have been reported and calibrated using in-house standards, calibrated against Vienna Standard Mean Ocean water (VSMOW) and Standard Light Antarctic Precipitation (SLAP) international waters. The choice of the in-house standards should minimize the difference between the standard values and the expected core values for Antarctica, to reduce the instrument's memory effect. Here we used the NEEM, Adelie ($\delta^{18}O$: -40.55 ± 0.05 ‰), and OC4 standards. We select the three last minutes of the standards measurements, for an injection of 25 minutes. Then we apply a linear regression between the standards measured values and their known values to correct data based on this deviation. To estimate the uncertainty on the standard measurements, we use Adelie as the check standard versus NEEM and OC4 standards, and find an average standard uncertainty of 0.01 ± 0.07 ‰ (1σ) on 8 days of measurements. Petteni et al. (2025) characterized the mixing at the melting head and in the tubings with a mixing length of 0.7 cm, which, combined with the noise level of the ®Picarro instrument used for the CFA analysis, yields an effective resolution at which a meaningful isotopic record can be disentangled of 1.6 cm. The resolution between the CFA data and the discrete measurements of the top part is thus comparable.

2.3 Chemistry analysis

The samples collected by the fraction collector were analysed at LSCE using ion chromatography to determine the concentrations of major ions in the ICORDA-LDC firn core, especially the sulphate concentration (SO_4^{2-}). Water samples were injected into two parallel Dionex ICS-5000+ ion chromatography systems, dedicated to the analysis of either cations or anions. For cation analysis, a 30 mMol MSA eluent flows at 0.17 mL/min through a CG16-4µm (2 × 50 mm) guard column and a CS16-4µm (2 × 250 mm) separation column. For anion analysis, a 55 mMol KOH eluent flows at 0.3 mL/min through an AG28-4µm (2 × 30 mm) guard column and an AS28-4µm (2 × 150 mm) separation column. The eluents then pass through Dionex DRS600 (2 mm) dynamically regenerated suppressors. The standard deviation for SO_4^{2-} measurements is estimated at 0.8 ppb from pooled variance of replicate samples.

2.4 Virtual Firn Core (VFC) model

We use the Virtual Firn Core (VFC) model, developed in Casado et al. (2020), based on the impact of precipitation intermittency on ice core records (Sime et al., 2011), and diffusion of a noise signal (Laepple et al., 2018). This model allows us to simulate what the firn cores at a site would be based on the precipitation amount, and the precipitation isotopic composition ($\delta^{18}O$ in this study). For each precipitation event, the model adds to the existing snowpack a new layer with a $\delta^{18}O$ value based on the precipitation isotopic composition and a thickness

https://doi.org/10.5194/egusphere-2026-871
Preprint. Discussion started: 4 March 2026

corresponding to the amount of snow, creating a depth profile by the superposition of the different layers corresponding to successive precipitation events.

To simulate the stratigraphic noise that disturb the isotopic signal, we follow Laepple et al. (2018) and Casado et al. (2020) and generate in parallel a temporally independent white noise, following a Gaussian distribution. The generated white noise is then applied to the virtual isotopic signal. The level of noise (%) describes the fraction of additional white noise in the signal. The noise scale determines the noise resolution, which corresponds to the smallest scale with potential isotopic variations. Here, we use a noise scale of 1 cm as in Laepple et al. (2018).

The white noise is added to the $\delta^{18}O$ profile as follows (Eq. 2):

$$\delta^{18}O_{noise} = (1-\xi)^{1/2} * \delta^{18}O_{ini} + \xi^{1/2} * SD_{\delta^{18}O} * \varepsilon \quad (Eq.2)$$

With $SD_{\delta 18O}$ the standard deviation of the initial isotopic signal ($\delta^{18}O_{ini}$) in the snow column, ε the white noise, and ξ the fraction of noise in the initial signal, between 0 and 1 for a noise level ranging from 0 % to 100 %.

In this study, we include into the VFC model the possibility of adding a surface mixing of the water isotopes. According to Ollivier et al. (in review), surface layers are indeed affected by mixing of the water isotopic signal through water vapor circulation in the first centimetres. We apply mixing in the model as a spatial moving average of the uncompacted snow isotopic profile, with a certain mixing scale.

Once the noise and mixing have been applied to the isotopic profile, the model calculates the column densification with depth, based on the density model of Herron and Langway (1980). Then, the model applies diffusion to the firn column, using the classical isotopic diffusion scheme (Johnsen, 1977, Johnsen et al., 2000, Gkinis et al., 2014, see Appendix B, Fig. B1). It corresponds to the diffusion of the water molecules in the porous space of the upper firn. The diffusion effect is calculated in the model by the diffusion length, a depth-dependent parameter calculated from temperature, accumulation rate, atmospheric pressure, and snow density (Laepple et al., 2018).

Finally, the firn isotopic signal is sampled with the same resolution as our observations, to allow comparison between the VFC model and the field data.

The power spectral density (PSD) was calculated for each VFC profile using the Thomson Multi-Taper method, as implemented in the nitime Python library (https://doi.org/10.25080/WXDN0820), with tapers of NW=2.5 normalized half-band width. For noise-inclusive reconstructions, we have shown an averaged spectrum corresponding to the average of a set of spectra obtained from ten emulated profiles in order to mitigate the random component introduced by the white noise distribution. Finally, we applied spectral smoothing on this averaged spectrum following the methodology of Münch and Laepple (2018). This method employs a Gaussian smoothing kernel whose width is proportional to the applied frequency, resulting in a constant smoothing width in logarithmic frequency space (Kirchner, 2005). A smoothing width of 0.05 in logarithmic units was selected.

2.5 LMDZ6-iso

Our simple virtual firn core model requires as inputs daily values of temperature, precipitation amount and precipitation-$\delta^{18}O$ to compute the isotopic signature of the snow. Here we use the atmospheric general circulation model equipped with water isotopes LMDZ6-iso (Laboratoire de Météorologie Dynamique model equipped with water isotopes, resolution 2.5° x 1.3°), developed by the Institut Pierre-Simon Laplace (see Risi et al., 2010,

https://doi.org/10.5194/egusphere-2026-871
Preprint. Discussion started: 4 March 2026

Hourdin et al., 2020). The simulations are nudged with the reanalysis ERA5 (see Hersbach et al., 2020), synchronizing observational data every 6 hours with real-time values of horizontal and vertical wind speeds, and temperature. Climate data for Antarctica are limited to the satellite era, since 1980. The model was evaluated for Antarctica in Dutrievoz et al. (2025) by comparing model outputs with field observations including surface snow and precipitation samples, temperature and water vapor continuous measurements, with a focus on Dumont d'Urville and Concordia stations. The model correctly depicts the temperature with a low bias for very cold temperature. The authors found that the isotopic simulation strongly depends on the supersaturation parameter λ. In our study, we chose the supersaturation parameter λ = 0.004 K-1 as for the Dome C site. With this parametrisation, we observe a bias of +2.6‰ for $\delta^{18}O$, which is corrected when we implement the precipitation-$\delta^{18}O$ data into the VFC model.

2.6 Synthetic data 2000 years

Since the nudged LMDZ6-iso simulations only go back to 1979, we generate synthetic monthly data of precipitation-$\delta^{18}O$, scaled with the precipitation intermittency, following the approach developed in Casado et al. (2020), here spanning 2000 years, corresponding to the age range covered by the firn cores.

The temperature signal is generated using a power-law relationship for the PSD of the climatic signal $S(f) \propto f^{-\beta}$ with β the scaling exponent. This parameter is supposed to reproduce the climate variability over longer periods than current climatic models (Huybers and Curry, 2006, Lovejoy and Schertzer, 2013) to ensure that the probability density distribution of the synthetic time series is closely matching the way the variability in the climate system is structured across time scales (Franzke et al., 2020).

According to the study of Münch et Laepple (2018) a value of β = 0.6 is realistic for Central Antarctica. Such a synthetic time series has spectral properties that are matching the ones we expect for the climatic signal in Central Antarctica over the last 2000 years, it is random by nature and there is no reason for the phase of the time series to match actual past temperature and isotopic composition variations, i.e. we do not expect features such as local maxima and minima to align with the isotopic signal in firn cores. This temperature time series can be converted into isotopic composition using a linear relationship of 0.5 ‰ $°C^{-1}$, which corresponds to the current observed slope for Dome C precipitation (Stenni et al., 2016, Dreossi et al., 2024).

To compute the effect of precipitation intermittency, without daily precipitation datasets, we add an amount of white noise to the synthetic climatic signal corresponding to the aliasing created by precipitation intermittency (Casado et al., 2020). The virtual core is simply calculated as the sum of the synthetic climatic signal and of this white noise signal with a PSD of 0.48 $‰^2$ m, representing the precipitation intermittency.

3 Results

3.1 Water isotopes

We present the $\delta^{18}O$ profiles of ICORDA-LDC (84 m long, as well as a zoom on the top 30 m) and Subglacior-LDC (30 m) firn cores (Fig. 2). Subglacior-LDC bag 4 is missing. The statistics (means and standard deviations) of the profiles are given in Table 1, on different scales, to compare the two profiles over the same lengths and distinguish the very porous upper part (first 3 metres) from the rest of the profile.

https://doi.org/10.5194/egusphere-2026-871
Preprint. Discussion started: 4 March 2026

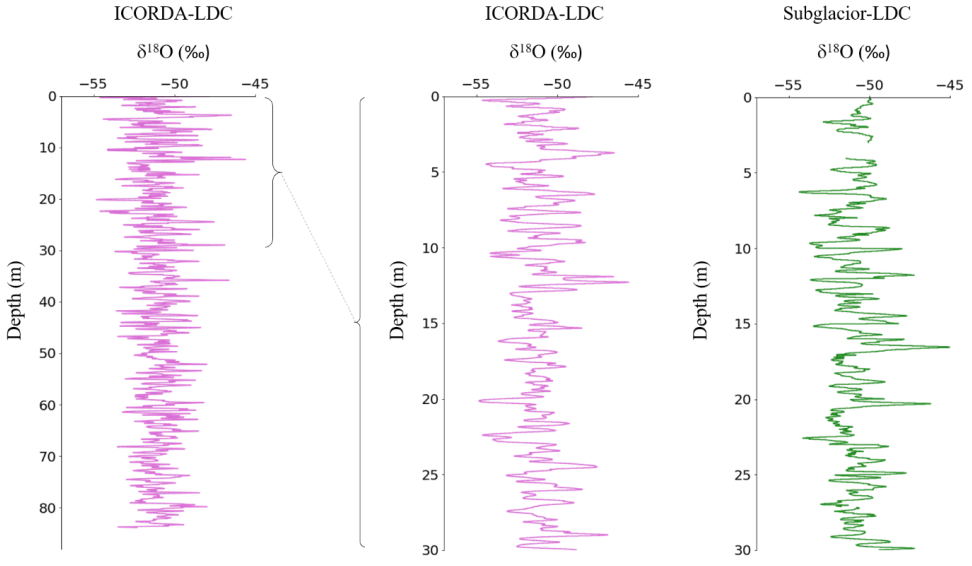

Figure 2 - $\delta^{18}O$ profiles of ICORDA-LDC (in pink) and Subglacior-LDC (in green) firn cores.

Table 1 - Means and standard deviations of ICORDA-LDC and Subglacior-LDC $\delta^{18}O$ profiles

	ICORDA-LDC		Subglacior-LDC	
	Mean	Standard deviation	Mean	Standard deviation
Depth: 0-84 m	-51.01	1.47	-	-
Depth: 0-30 m	-51.10	2.14	-50.89	1.76
Depth: 0-3 m	-51.21	0.68	-50.67	0.60
Depth: 3-30 m	-51.10	2.15	-50.90	1.82

The $\delta^{18}O$ mean value for ICORDA-LDC is lower than for Subglacior-LDC, with respective values of -51.10 ‰ versus 50.89 ‰ on the top 30 m of the cores. The origin of this offset is not clear, but can be interpreted either as evidence of the preferential evaporation of lighter isotopes within the bag during prolonged storage of Subglacior-LDC. The standard deviation for ICORDA-LDC is higher than for Subglacior-LDC (2.14 ‰ versus 1.76 ‰ over 30 m, or 2.15‰ versus 1.82‰ when removing the 3 m top part), which may be due to sampling resolution or increased diffusion for Subglacior-LDC during the storage. Since the ICORDA-LDC and Subglacior-LDC were drilled a few years apart, there is a depth and time shift between the profiles, and it is necessary to define the chronology to align them.

3.2 Chemistry and construction of chronology

Here we present the sulphate profiles for ICORDA-LDC and Subglacior-LDC (Fig. 3). The profiles exhibit a noisy baseline level between 50 and 100 ppb with highly variable intensity peaks that can reach over 1000 ppb. By comparing the two profiles, we identify common peaks for both firn cores, although the intensities of these peaks differ. The peaks at depth around 2 m, 13 m, 29 m, and 37 m are particularly noticeable on both profiles, with a

https://doi.org/10.5194/egusphere-2026-871
Preprint. Discussion started: 4 March 2026

slight offset due to the drilling schedule. These sulphate peaks correspond to large volcanic events and the subsequent deposition of volcanic material on the surface of Antarctica, some of which have been identified and dated at Dome C (DC) (Gautier et al., 2016, 2018, 2019, dataset available here, DOI: https://doi.org/10.1594/PANGAEA.895169). We transfer this previous peak identification at DC to the LDC firn cores to establish the ICORDA-LDC and Subglacior-LDC chronologies. We estimate the mean accumulation between each volcanic tie point by summing the firn mass, based on the density of each bag measured in the field (Appendix A, Table A1), between two volcanic horizons. We then compute the number of years within each bag i, Δt_i, according to the total mass of the bag and the mean annual accumulation of the corresponding period (acc_{period} in mm water equivalent per year mmwe.yr^{-1}, or kg.m^{-2}.yr^{-1}) (Eq. 3):

$$\Delta t_i = \frac{\rho_i \, dz_i}{acc_{period}} \quad (Eq. 3)$$

ρ_i (kg.m^{-3}) and dz_i (m) refer to the density and the length of each bag.

The age of a bag t_{bag} is the cumulative time span from the first most confident tie point t_0 (Eq. 4).

$$t_{bag} = t_0 - \sum_{i=0}^{bag} \Delta t_i \quad (Eq. 4)$$

Finally, we find that the 84 meters of firn of ICORDA-LDC cover ~2195 years, and the 42 meters of Subglacior-LDC cover ~553 years. Based on our results, the accumulation rate at LDC is estimated at approximately 24 mmwe.yr^{-1}, comparable to the value of Chung et al. (2025) for the top 80 meters of firn.

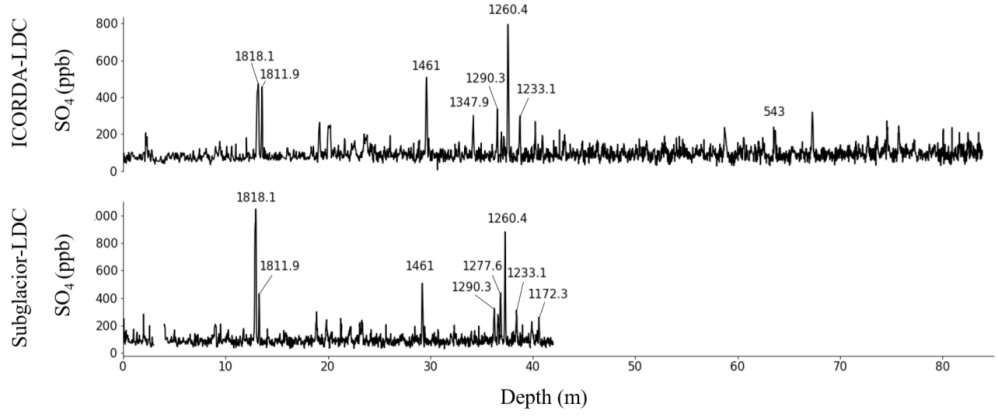

Figure 3 - Sulphates records in ICORDA-LDC and Subglacior-LDC firn cores. The largest sulphates peaks were identified as volcanic eruption proxies, and dated based on the DC stack (Gautier et al., 2018, 2019)

The common chronology allows us to compare the $\delta^{18}O$ profiles between ICORDA-LDC and Subglacior-LDC (Fig. 4). No consistent structures appear between the two profiles once they are aligned. We explain this by the very local effect of stratigraphic noise, already pointed out by (Fisher et al., 1985, Ekaykin et al., 2002, Laepple et

https://doi.org/10.5194/egusphere-2026-871
Preprint. Discussion started: 4 March 2026

al., 2018). In this context, to extract a meaningful climatic signal from ice cores records without the imprint of both precipitation intermittency and stratigraphic noise, it is necessary to either combine a large number of cores or consider longer time scales (Münch and Laepple, 2018). As the signal-to-noise ratio (SNR) in a single firn core in Central Antarctica is around 0.1 at the interannual scale (Münch and Laepple, 2018), to obtain a SNR of 1, it is necessary to average roughly 10 cores (as the SNR scales with the number of cores) (Casado et al., 2023). Here, with only two ice cores, our data series could thus not be used yet to extract a meaningful climatic signal on the overlapping period. We also note that no significant signal emerges following major volcanic eruptions.

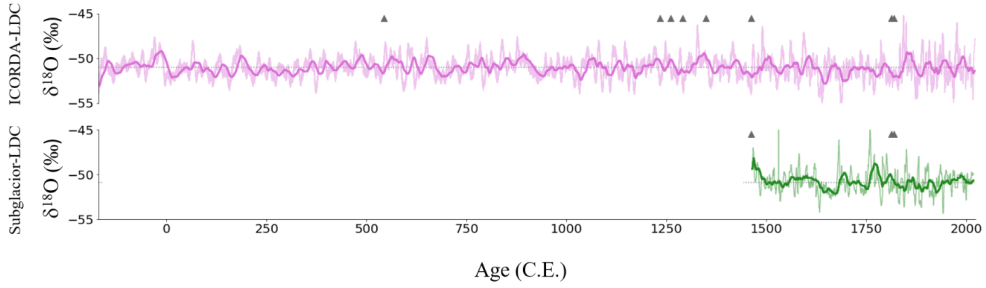

Figure 4 - $\delta^{18}O$ profiles in ICORDA-LDC (in pink) and Subglacior-LDC (in green) firn cores aligned on a common chronology based on volcanic tie points. The grey triangles indicate the volcanic tie points used for each core, the bold curves represent the moving average of the profiles over 20 years and the dotted lines show the mean value of each series.

3.3 Virtual Firn Core (VFC) construction

Despite the alignment of the two firn cores on the same age scale, the isotopic profiles do not show any clear correlation (Fig. 4) (corr = -0.02, p-value > 0.05). We present outputs of the VFC model on two different scales, the 3 m top-scale and 80 m long-scale, in order to study the effects of stratigraphic noise and mixing occurring at the surface, as well as the effect of diffusion that intensifies deeper. The upper 3-meters correspond to the last 30-40 years which is the time covered by satellite data and we can thus use daily meteorological data from LMDZ6-iso forced by reanalyses for VFC construction. When we work on the scale of the whole firn (80 m), we use the 2,000 years synthetic data. A comparison of the 3 m top-scale inferred from the monthly synthetic data and monthly LMDZ6-iso data is displayed in the Supplementary Material (Appendix B, Fig. B2).

https://doi.org/10.5194/egusphere-2026-871
Preprint. Discussion started: 4 March 2026

3.3.1 VFC without noise nor mixing

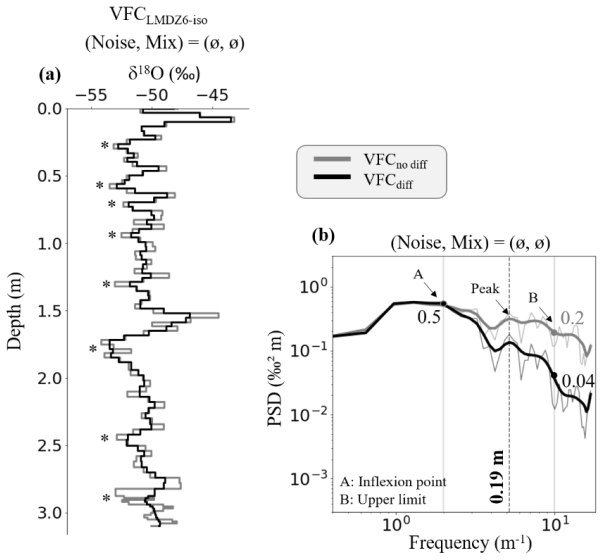

Figure 5 - VFC $\delta^{18}O$ profile (a) before (in grey, $VFC_{no\ diff}$) and after (in black, VFC_{diff}) diffusion, built from LMDZ6-iso daily climatic data on the 3 m top-scale. No noise nor mixing has been added to the model (Noise, Mix) = (ø, ø). The stars indicate the minima used to count cycles in the diffused signal. The PSD of the signals is given by the spectra (b), with the smoothed signals in bold. A small peak in the frequencies is indicated by the vertical dashed line. The two solid lines in grey delimit the spectral domain where we evaluate the attenuation of the high frequencies after the inflection point (corresponding to Frequency = $2 m^{-1}$).

On the 3 m top-scale VFC $\delta^{18}O$ emulation without additional noise nor mixing, the $\delta^{18}O$ variability lies between -45 and -55‰ (Fig. 5). The frequency of the cycles is higher just below the surface, with five cycles between 0 and 1.5 meters deep, and conversely, wider cycles deeper (only three cycles between 1.5 and 3 meters deep). The diffusion effect slightly reduces the amplitude of the signal and remove the high frequency variability (short cycles of small amplitude) as observed when comparing the VFC $\delta^{18}O$ signal with and without diffusion (Fig. 5).

Both diffused and non-diffused signal spectra exhibits a flat distribution for frequencies between 1 m^{-1} and 2 m^{-1} (corresponding to a period of 1 m to 50 cm), followed by a pronounced decrease in power at higher frequencies. We refer to this threshold of 2 m^{-1} as the inflection point of the spectra. We then define the spectral slope as the attenuation slope of the high frequencies between the inflection point and an arbitrary upper limit set at Frequency = 10 m^{-1} (corresponding to 10 cm). This slope is steeper after diffusion, going from a PSD value of 0.5 ‰² m at the inflection point, to 0.04 ‰² m at the upper frequency limit, compared to 0.2 ‰²m before diffusion, highlighting how the diffusion cuts off the high frequencies. The spectra show a small peak corresponding to a period of 19 cm, which may be compared to the apparent 20 cm cycle of diffusion acting on noise-dominated input, shown by Laepple et al. (2018).

On the 80 m long VFC $\delta^{18}O$ emulation without additional noise nor mixing (Fig. 6), constructed from synthetic climate data, the effect of diffusion on the $\delta^{18}O$ profile is striking. The $\delta^{18}O$, which varies between approximately

https://doi.org/10.5194/egusphere-2026-871
Preprint. Discussion started: 4 March 2026

-56 and -46‰ before diffusion, is reduced to variations between -52 and -50‰ after diffusion. We calculate the spectra over three windows along the simulated profile to see how the frequency distribution evolves with depth: window 1 = [depth: 5 to 10 m]; window 2 = [depth: 40 to 45 m]; and window 3 = [depth: 75 to 80 m]. On the spectra, the spectral slope remains relatively flat for the non-diffused signal, as expected from the signal input, which contains a significant part of intrinsic white noise, while the spectral slope after diffusion displays a PSD decrease from 0.2 to 0.001 ‰² m in window 1, and a dramatic drop at greater depths in windows 2 and 3 (from 0.08 to <0.00002 ‰² m).

https://doi.org/10.5194/egusphere-2026-871
Preprint. Discussion started: 4 March 2026

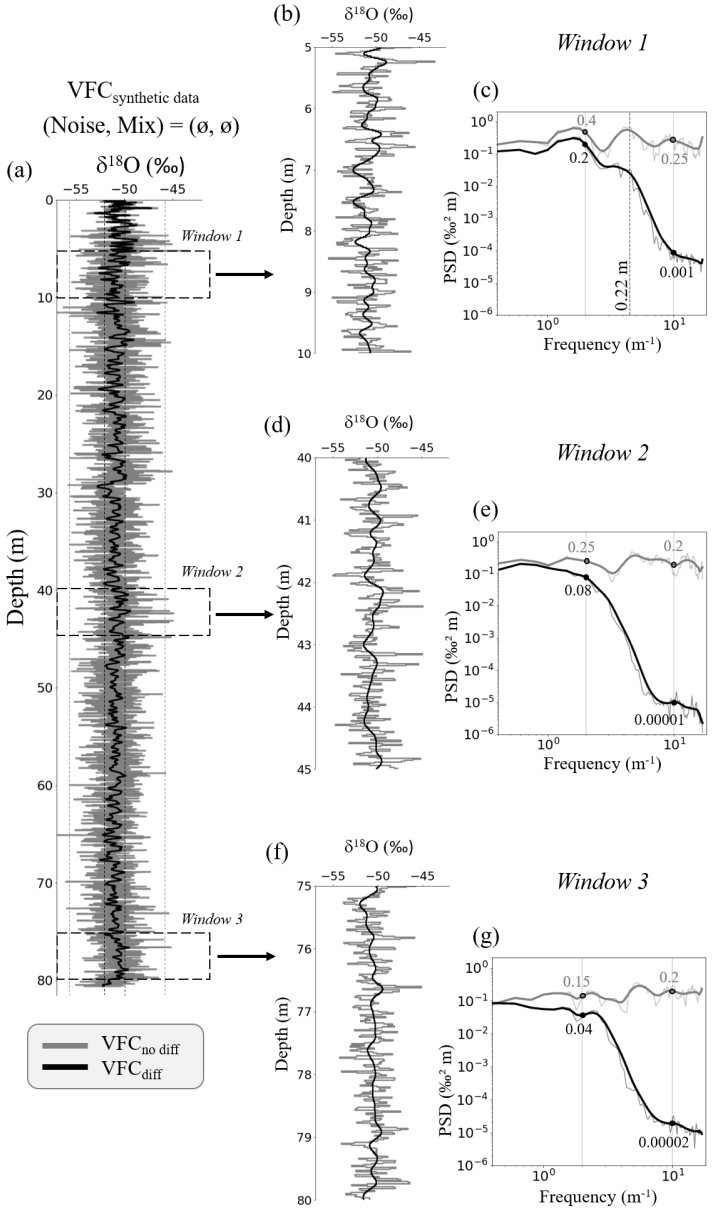

Figure 6 - VFC $\delta^{18}O$ profile before (in grey, $VFC_{no\ diff}$) and after (in black, VFC_{diff}) diffusion, built from monthly synthetic climatic data (a) on the 80 m long-scale. No noise nor mixing has been added to the model (Noise, Mix) = (ø, ø). We display three profile sections between (window 1, b) 5-10m, (window 2, d) 40-45m, (window 3, f) 75-80m depth and their spectra on the right (c, e, g, respectively). The two solid lines in grey delimit the spectral domain where we evaluate the attenuation of the high frequencies after the inflection point (corresponding to Frequency = $2m^{-1}$).

https://doi.org/10.5194/egusphere-2026-871
Preprint. Discussion started: 4 March 2026

3.3.2 Addition of noise and mixing

We evaluate the effect of noise and mixing on the simulation by performing sensitivity tests with varying noise levels ranging from 0 to 90 %, and mixing length ranging from 0 to 16 cm (Appendix B, Fig. B3, B4). The increase in noise implemented alone in the VFC model (without mixing) has only a limited effect on the spectral slope, except for extreme values of noise (90 %) which lower the PSD at the inflection point (Fig. 7 a, c). The addition of noise also slowly dampens the frequency peak at 19 cm, hardly identifiable beyond 50 % of noise. By contrast, the addition of surface mixing in the VFC model strongly impacts the signal (Fig. 7 b, d). Even though the inflection point remains at 0.5‰² m, the spectral slope drops dramatically at high frequencies. The frequency peak at 19 cm remains visible up to a mixing scale of 12 cm. Therefore, mixing appears to be a first order factor in modulating the VFC signal in the 3 m top-scale, while noise has only a marginal effect as classicaly implemented (Laepple et al., 2018, Casado et al., 2020).

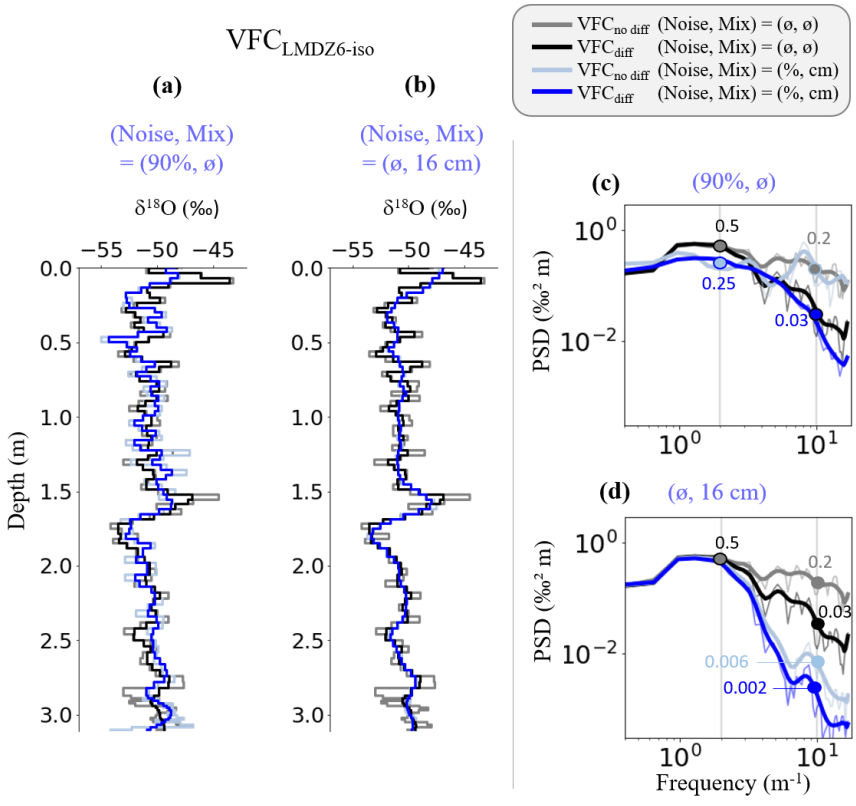

Figure 7 - VFC $\delta^{18}O$ profiles built from LMDZ6-iso daily climatic data on the 3 m top-scale. In grey the profile before diffusion, and in black the profile after diffusion, both without noise nor mixing effect. In light blue and dark blue respectively the non-diffused and diffused profile with (a) 90 % of noise (Noise, Mix) = (90 %, ø), (b) mixing with a 16-cm mixing scale (Noise, Mix) = (ø, 16 cm). We display the signal spectra on the right (c, d, respectively), the light blue and dark blue thin lines correspond to the average spectra for ten emulations each, and the bold lines correspond to the smoothed spectra.

https://doi.org/10.5194/egusphere-2026-871
Preprint. Discussion started: 4 March 2026

On the 80 m long-scale, the addition of noise (Fig. 8 a, c, e) does not appear to have any significant effect on the non-diffused or the diffused $\delta^{18}O$ profiles and spectra. It also does not modify the amplitude and frequency of the simulated signal.

The addition of mixing (Fig. 8 b, d, f), reduces the high frequencies of the non-diffused signal (PSD values from 0.3 to 0.01 ‰² m compared to 0.2 ‰² m at the upper frequency limit without mixing) but has no visible impact on the diffused signal (spectral slope from 0.05 to 0.00001 ‰² m with and without mixing).

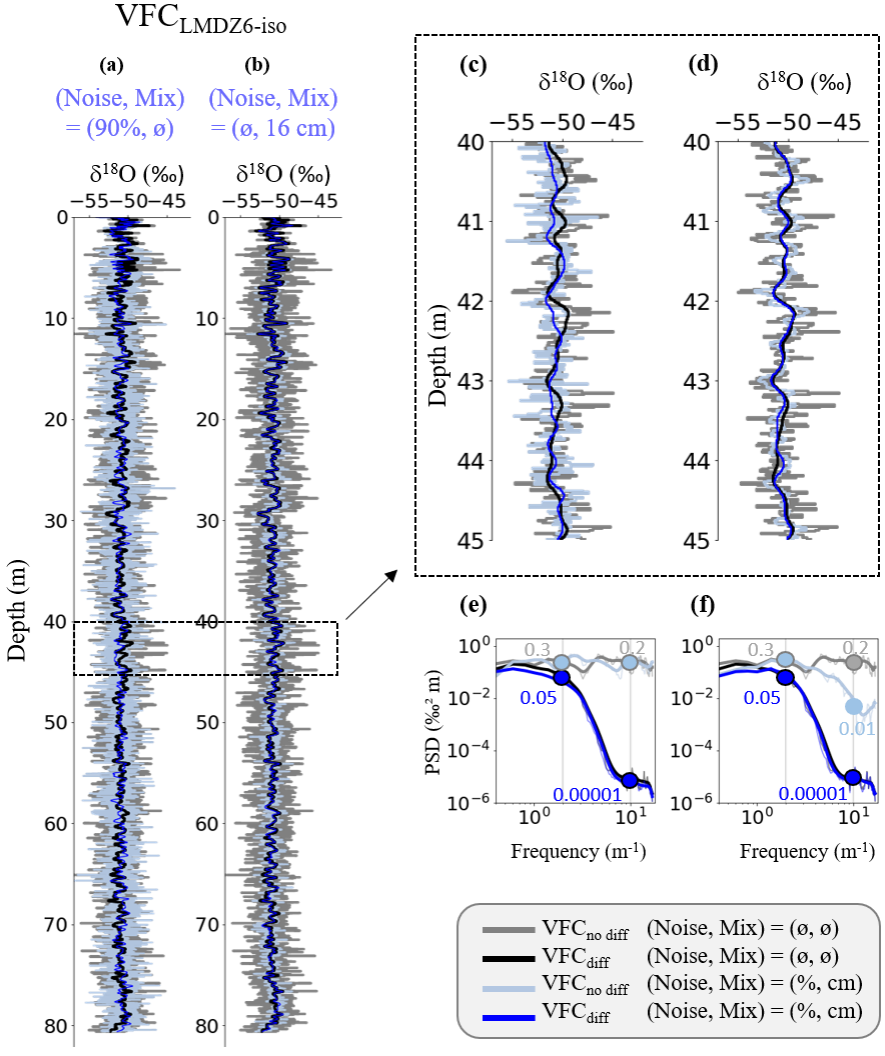

Figure 8 - VFC $\delta^{18}O$ profiles built from monthly synthetic climatic data on the 80 m long-scale. In grey the profile before diffusion, and in black the profile after diffusion, both without noise nor mixing effect. In light blue and dark blue respectively the non-diffused and diffused signals with (a) 90 % of noise (Noise, Mix) = (90 %, ø), (b) mixing with a 16-cm mixing scale (Noise, Mix) = (ø, 16 cm). We display a zoom section of the profiles between (c, d, respectively) 40-45 meters depth and the spectra of each below (e, f, respectively). The light blue and dark blue thin lines correspond to the average spectra for ten emulations each, and the bold lines correspond to the smoothed spectra.

https://doi.org/10.5194/egusphere-2026-871
Preprint. Discussion started: 4 March 2026

4 Discussion

4.1 Data-model comparison

We compare ICORDA-LDC and Subglacior-LDC with the VFC model results, over the 3 m top-scale (Fig. 9) and over the whole core lengths (Fig. 10). The depth scale for Subglacior-LDC was recalculated using the year of the top of ICORDA-LDC as the reference surface.

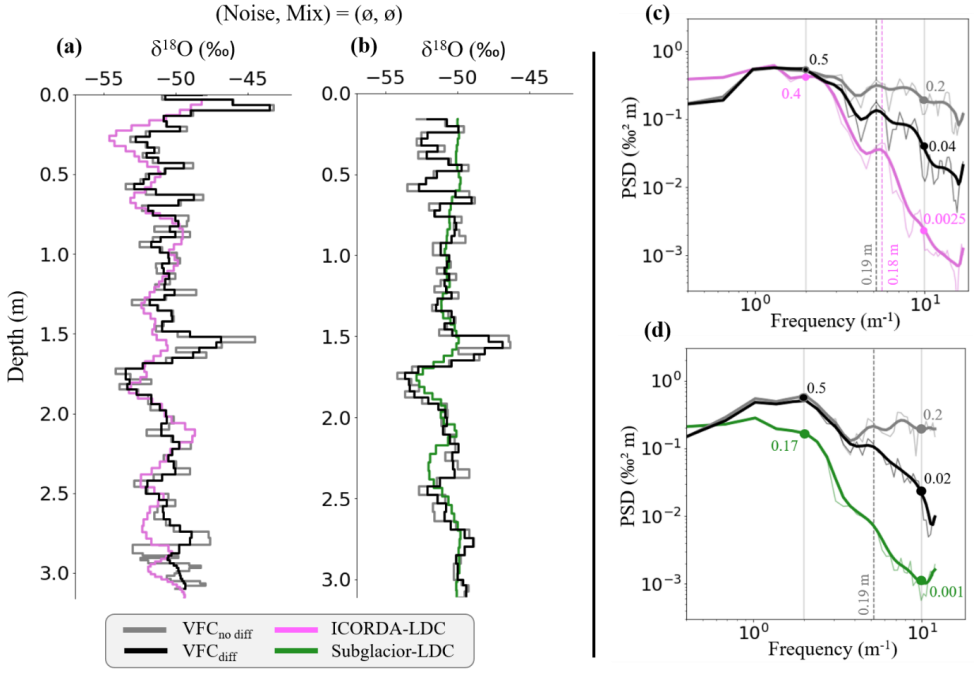

Figure 9 - VFC $\delta^{18}O$ profiles built from LMDZ6-iso daily climatic data, before (in grey) and after (in black) diffusion, without noise and without mixing, compared with ICORDA-LDC $\delta^{18}O$ profile (a, in pink) and Subglacior-LDC (b, in green) on the 3 m scale. Signal spectra are displayed on the right (c, d, respectively). The dashed lines highlight the frequencies peaks and the grey solid lines delimit the spectra slopes.

https://doi.org/10.5194/egusphere-2026-871
Preprint. Discussion started: 4 March 2026

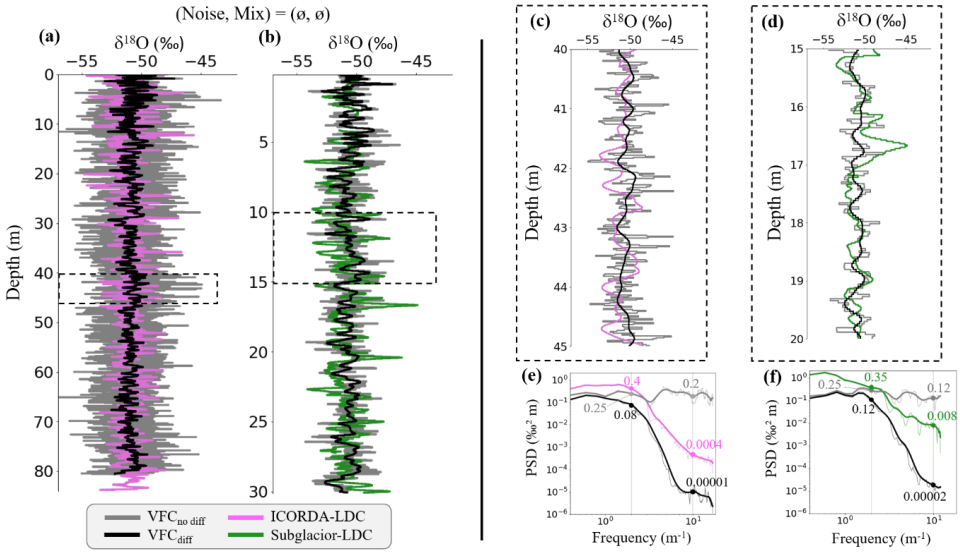

Figure 10 - VFC $\delta^{18}O$ profiles (a, b) and sections (c, d) built from monthly synthetic climatic data, before (in grey) and after (in black) diffusion, without noise and without mixing, compared with ICORDA-LDC $\delta^{18}O$ profile (a, c, in pink) and Subglacior-LDC (b, d, in green) on the long scale. Signal spectra are displayed below (e, f, respectively). The grey solid lines delimit the spectra slopes.

The $\delta^{18}O$ profiles simulated from the VFC model without noise and without mixing do not match the firn cores data, at both scales (3 m top-scale and 80 m long-scale).

On the 3 m top-scale, the cycles in the firn $\delta^{18}O$ profiles are fewer and wider than in the VFC. In addition, the $\delta^{18}O$ signal is particularly flat between 0 and 1.5 m for Subglacior-LDC, even compared to ICORDA-LDC. On the spectra, we note that the PSD at all frequencies is higher for the VFC than for the firn data. The VFC spectral slope after diffusion shows a decrease from 0.5 ‰² m to 0.04 or 0.02 ‰² m (depending on the sampling resolution), while ICORDA-LDC shows a spectral slope from 0.4 ‰² m to 0.0025 ‰² m and Subglacior-LDC from 0.17 ‰² m to 0.001 ‰² m. The frequency peak identified previoulsy at 19 cm in the VFC spectrum is also visible in the ICORDA-LDC spectrum at 18 cm, but not in the Subglacior-LDC spectrum.

On the contrary, on the long-scale (80 m for ICORDA-LDC, 30 m for Subglacior-LDC) the PSD at all frequencies for the diffused VFC is lower than for the observations. The lower PSD in the VFC is associated with two different effects: a lack of low-frequency variability (which could be due to an underestimation of the interannual signal in the synthetic data as well as missing stratigraphic noise for instance) and an apparent over-estimation of the low-pass filter associated with excessive diffusion of the signal at high frequency for depth below 5 m.

4.2 Quantifying impact of mixing and noise at LDC

For the 3 m top-scale, mixing at the surface improves the match between the VFC outputs and the observations by removing the high frequency variability. We conduct sensitivity tests by varying the mixing scale between 0 and

https://doi.org/10.5194/egusphere-2026-871
Preprint. Discussion started: 4 March 2026

12 cm. Because noise level is also a component which may improve the model-observation comparison, we also run test with noise levels (% noise) between 0 and 90 %. We show a few data-model comparisons in the Supplementary Material (Appendix B, Fig. B5). For each sensitivity test, we evaluate the difference between the VFC model output and ICORDA-LDC measured series by calculating the Root Mean Square (RMS) score (Eq. 5) from the differences in PSD at the inflection point (A) and at the upper limit point (B), (Fig. 11). We calculate the RMS score using the following formula:

$$RMS\ score = \sqrt{\frac{\Delta PSD(A)^2 + \Delta PSD(B)^2}{2}} \quad (Eq.5)$$

A low RMS score indicates good agreement between the model and the data. Conversely, a high RMS score indicates a poor model data agreement.

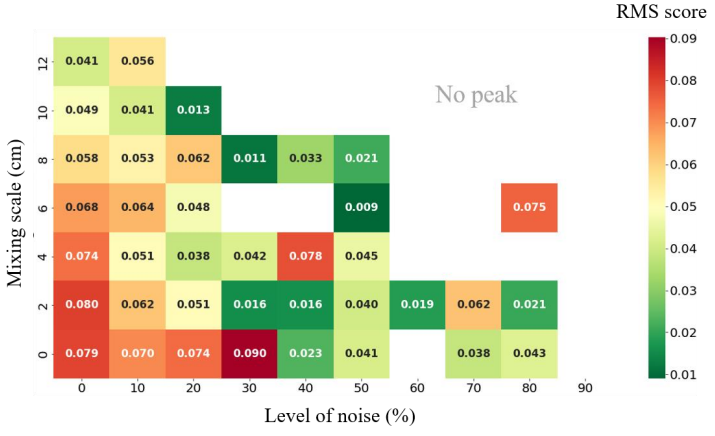

Figure 11 – Model-observations RMS score for the various sensitivity tests of the VFC model, with a noise level varying from 0 to 90 % and a mixing scale ranging from 0 to 12 cm. Missing scores correspond to simulations where the frequency peak at 18-19 cm does not appear and which are thus excluded. A low RMS score (green) indicates a good match between the model and the observations, while a high RMS score (red) indicates that the model-observation fit is poor.

As displayed in Fig. 11, the best combinations to optimize the model-data fit are (Noise, Mixing) = (50 %, 6 cm) and (Noise, Mixing) = (30 %, 8 cm). A third combinations (Noise, Mixing) = (20 %, 10 cm) gives close results but such a long mixing scale is not consistent with field observations and values obtained by Ollivier et al. (in review) and is thus rejected. By combining the RMS score with a direct visual comparison of the spectra (Appendix B, Fig. B6), we select the combination (Noise, Mixing) = (30 %, 8 cm) as the best noise and mixing setting for the model to reproduce the observations (Fig. 12).

https://doi.org/10.5194/egusphere-2026-871
Preprint. Discussion started: 4 March 2026

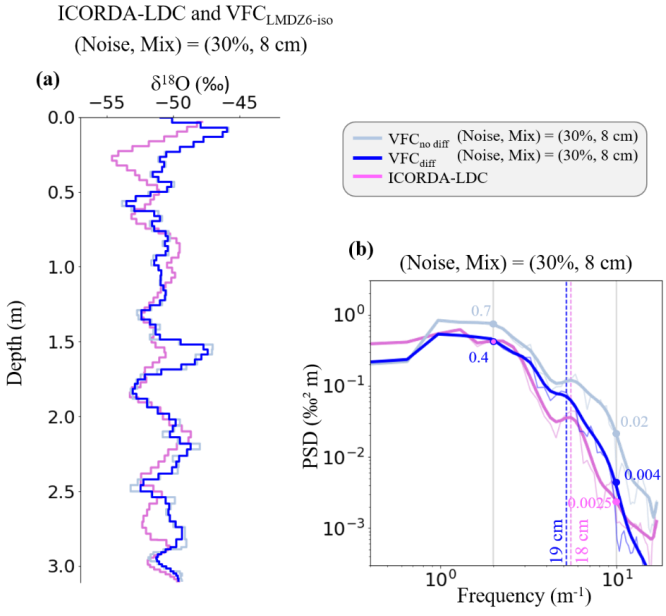

Figure 12 - VFC δ^{18}O profiles (a) built from LMDZ6-iso daily climatic data, before (in light blue) and after (in dark blue) diffusion, with 30 % noise and mixing on a 8-cm mixing, compared with ICORDA-LDC δ^{18}O profile (in pink) on the 3 m top-scale. Signal spectra (b) are displayed on the right. The light blue and dark blue thin lines correspond to the average spectra for ten emulations each, and the bold lines correspond to the smoothed spectra. The dashed lines highlight the frequencies peaks and the grey solid lines delimit the spectra slopes.

Based on surface and sub-surface water isotope data (top 6 cm), Ollivier et al. (in review) proposed a mixing layer of 4 cm at DC and imputed it to changes in wind strength and snow properties. Our study suggested that 4 cm is not sufficient to explain the observed water isotopes variability over the top 3 m at LDC. The isotopic variability with a 6 cm or 8 cm mixing layer needed for our data-model comparison is also in agreement with Ollivier et al. (In review).

Neither our best settings nor any other combination of noise and mixing can reproduce well the profile and spectra of Subglacior-LDC, which displays a particularly flat signal from 0 to 1.5 m depth (Fig. 12, with (Noise, Mixing) = (30 %, 8 cm)). Furthermore, the Subglacior-LDC profile is very different from the ICORDA-LDC profile despite the proximity of the two boreholes. We suspect that the isotopic signal underwent a transformation between core drilling and analysis. Dallmayr et al. (2025) indeed show that water isotope distribution in firn samples is particularly sensitive to the storage time in cold rooms at -20°C, implying additional diffusion. Subglacior-LDC core has been stored for five years before analysis, and this long storage time is thus expected to have affected the very low-density material in the first meters below the surface, where we observe a flat isotopic signal. Based on Dallmayr et al. (2025), we implement an additional storage diffusion in the VFC model as follows (Eq. 6):

$$\sigma^2_{drilling} = \sigma^2_{measurement} + \sigma^2_{storage} \quad (Eq.\,6)$$

https://doi.org/10.5194/egusphere-2026-871
Preprint. Discussion started: 4 March 2026

with $\sigma_{storage}$ = 5.6 cm for five years of storage. Even when adding this storage diffusion, the VFC $\delta^{18}O$ profile never matches the shape displayed by Subglacior-LDC with large remaining differences in spectra slopes (0.25 versus 0.17 and 0.0004 versus 0.001 ‰² m, Fig. 13b). We note that Dallmayr et al. (2025) estimated $\sigma_{storage}$ at a depth between 2.40 and 3.40 m, i.e. shifted slightly deeper than our 0-3 m depth interval. Because open porosity is larger closer to the surface, we expect $\sigma_{storage}$ from Dallmayr et al. (2025) to be underestimated for our application. A larger value of $\sigma_{storage}$ would improve the agreement between the measured and the simulated $\delta^{18}O$ profiles. This storage effect is minimized for ICORDA-LDC core due to the short storage time (a few months) prior to isotopic measurements.

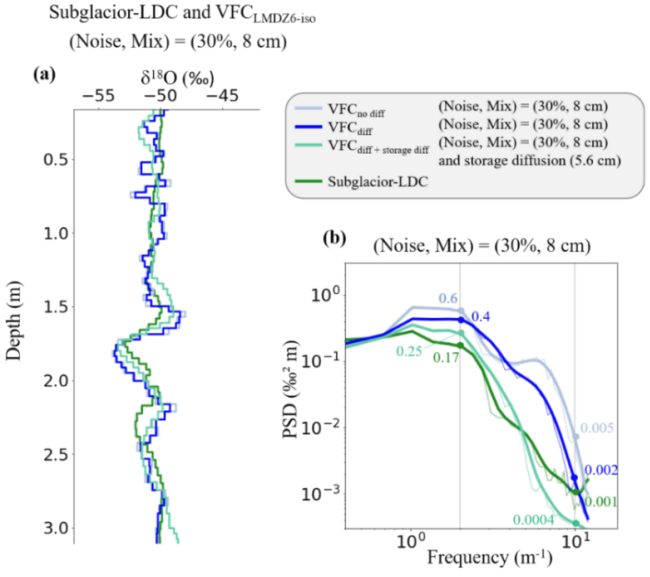

Figure 13 - VFC $\delta^{18}O$ profile (a) built from daily LMDZ6-iso climatic data, before (in light blue) and after (in dark blue) diffusion, with 30 % noise and mixing on a 8-cm mixing scale (Noise, Mix) = (30 %, 8 cm), and adding storage diffusion (in turquoise) as defined by Dallmayr et al. (2025) for five years of storage at -20°C (Noise, Mix, Storage diff) = (30 %, 8 cm, 5.6 cm), compared with Subglacior-LDC $\delta^{18}O$ profile (in dark green) on the 3 m top-scale. Signal spectra (b) are displayed on the right. The turquoise, light blue and dark blue thin lines correspond to the average spectra for ten emulations each, and the bold lines correspond to the smoothed spectra. The grey solid lines delimit the spectra slopes.

Back to the 80 m long-scale, the addition of noise and mixing is not expected to improve the reconstruction, as the signal is already too dampened by the diffusion and the PSD values are too low at all frequencies. The profiles and spectra for (Noise, Mix) = (30 %, 8 cm), are presented in the Supplementary material (Appendix B, Fig. B7, B8), but overall retain the same spectral slopes with and without noise and mixing. The main source of discrepancy between model and data is in the overestimation of diffusion.

4.3 Implications for future VFC models

Our study shows that the classically tuned VFC model cannot reproduce the $\delta^{18}O$ variability in the firn at LDC. We focus on two depth scales that highlight two distinct issues: the 3 m top-scale where the $\delta^{18}O$ variability

https://doi.org/10.5194/egusphere-2026-871
Preprint. Discussion started: 4 March 2026

simulated by the VFC model is exaggerated, with an overrepresentation of high frequencies, which can be addressed by implementing mixing near the surface; and the 80 m long-scale where the VFC signal is too diffused compared to the measured profiles. No tuning of the VFC model based on classical diffusion calculations allows us to reproduce the LDC firn $\delta^{18}O$ profiles in both the upper part where more diffusion would be required, and at depth where less diffusion would be needed.

Our firn data are not the only ones to suggest a too strong diffusion in reconstructions based on Johnsen's diffusion model. Van der Wel et al. (2015) monitored the isotopic diffusion of a layer of artificial snow when buried annually in Greenland and found less intense diffusion in the subsurface than predicted in the classical diffusion model. Touzeau et al. (2018) showed that the $\delta^{18}O$ semi-amplitude in shallow 80 m cores from GRIP (in Greenland) was lower than that modelled. There is thus convergence across these studies and our results, challenging the correct quantification of the diffusion which may be too strong at some depths but not sufficient to produce the correct signal near the surface.

In his foundational study, Johnsen (1977) initally mentioned two processes to explain the variability of water isotopes and signal attenuation in the firn: diffusion and barometric pumping. He dismissed the barometric pumping hypothesis, citing the presence of "frequent impermeable ice and crust layers in Dye 3 core (south Greenland)" that would prevent the process from occurring, leaving the diffusion as the preferred hypothesis. Yet, ice and crust layers are not very common in many very cold and dry sites, such as in Central Antarctica. However, only the diffusion hypothesis was considered in the large majority of subsequent studies.

Neuman and Waddington (2004) developed an alternative model based on the barometric pumping hypothesis and suggest distinguishing between the first few meters of firn below the surface, affected by barometric pumping, and deeper firn. For these authors, diffusion alone cannot be responsible for signal attenuation, and they involve barometric pumping, linked to the material tortuosity. Complementary studies based on inert gas isotopic composition in firn or bubbles trapped in ice cores support ventilation or air advection in the top of the firn at Dome C, this process being often referred to as the rectifier effect (Harris-Stuart, 2024, Morgan et al., 2022, Grimmer et al. 2025).

The surface firn ventilation hypothesis is probably more relevant at LDC than for Greenland for which Johnsen developed his firn diffusion formulation. Indeed, temperatures are much colder on the East Antarctic Plateau, preventing the layers in the firn from melt-refreezing. In addition, the texture of the firn in the upper 3 meters at LDC was so fragile and porous that it prevented the cutting of CFA bars. This empirical processing evidence suggests that this material is very conducive to air ventilation, and thus favourable to exchanges between the water vapor and the grains. In addition to firn ventilation, the low accumulation at LDC leads to prolonged exposure of snow at the surface, which may also permit direct mixing of snow grains lying at the surface under the influence of the wind. Thus, snow surface reworking is expected due to direct action of the wind on the surface and migration of micro-dunes, with effects on a multi-centimetre scale. Both snow reworking and firn ventilation can induce mixing of water isotopes at the surface and below the surface, and none of these processes are incorporated in diffusion-only models.

https://doi.org/10.5194/egusphere-2026-871
Preprint. Discussion started: 4 March 2026

In our study, we propose improving the VFC model by adding a mixing parameter to improve the reconstruction of firn $\delta^{18}O$ profile, in order to represent the effects of barometric pumping and surface reworking. This improvement of the model in the upper part does however not correct the discrepancies between firn measurements and virtual profiles at deeper depths, where the implementation of diffusion using the classic approach supresses the high frequencies signal. Diffusion is necessary, as predicted by Johnsen (1977), because our observations lie between the non-diffused and the diffused signals, but its intensity is stronger than observed and needs to be re-evaluated.

5 Conclusions

This work aims to characterize isotopic processes in the firn at LDC. We present the first dated water isotopic profiles over the top 80 m at the LDC site, the drilling site of BELDC, and compare a VFC model to better understand the surface processes influencing the variability of water isotopes in the firn.

In the first few meters below the surface, we demonstrate the need to consider a mixing process, involving a layer of approximately 8 cm, in addition to diffusion, to smooth the isotopic variability. This mixing probably results from barometric pumping and surface reworking. Compared to the mixing process, the addition of stratigraphic noise only marginally improves the data-model agreement. At the deeper scale (80 m), the comparison between the model and the data highlights an incorrect estimation of diffusion, which is too strong according to the classical approach, and from a perspective we stress the need to re-assess the intensity of firn diffusion at LDC to match the signal attenuation observed in firn cores.

At the end, we draw attention to the importance of measuring water isotopes in firn quickly after drilling, so before that additional diffusion occurs during the cores' storage in cold rooms at -20°C, as it was the case in the Subglacior-LDC top.

https://doi.org/10.5194/egusphere-2026-871
Preprint. Discussion started: 4 March 2026

Author contributions

ES and AL wrote the manuscript with contributions from all co-authors. The CFA data from ICORDA-LDC were obtained through the work of EF, ES and TC. TC and EF generated the ICORDA-LDC chromatography data. The discrete isotope measurements for Subglacior-LDC and top ICORDA-LDC were carried out by BM, and the chromatography measurements by EG. The VFC model was largely based on and improved from MC's model with the help of AO. ND and CA provided the LMDZ6-iso climate model data for LDC. The interpretation of the results was mostly performed by ES, AL, MC and VMD.

Competing interests

The authors declare that they have no conflict of interest.

Financial support/ Acknowledgements

This research has received funding from the European Research Council under the European Union Horizon 2020 Excellent Science program (H2020/20192024)/ERC grant agreement no. 817493 (ERC ICORDA). This study has also been supported by ANR Toward Beyond-EPICA (ToBE), by the Centre à l'énergie atomique et aux énergies alternatives (CEA), by the Centre National de la Recherche Scientifique (CNRS), and by the Institut Pierre-Simon Laplace (IPSL). The collection of data would have not been possible without the logistical support of the Institut Polaire français Paul-Emile Victor (IPEV, project n°1250).

Acknowledgements

The field work was supported by the F2G drilling platform for drilling the two firn cores. We sincerely acknowledge the drilling team consisting of Anaïs Orsi, Roxanne Jacob, Gregory Teste and Philippe Possenti. We would also like to thank Maria Hörhold and Jean Jouzel for interesting discussion on the issues raised by this research.

https://doi.org/10.5194/egusphere-2026-871
Preprint. Discussion started: 4 March 2026

References

Barbante, C., and the Beyond Epica team (2025). Beyond EPICA–Oldest Ice Core: Insights from a 1.2-Million-Year-Old Climate Record. *EGU 2025*. https://meetingorganizer.copernicus.org/EGU25/EGU25-10358.html

Berends, C. J., Köhler, P., Lourens, L. J., & Van De Wal, R. S. W. (2021). On the Cause of the Mid-Pleistocene Transition. *Reviews of Geophysics*, *59*(2), e2020RG000727. https://doi.org/10.1029/2020RG000727

Casado, M., Hébert, R., Faranda, D., & Landais, A. (2023). The quandary of detecting the signature of climate change in Antarctica. *Nature Climate Change*, *13*(10), 1082–1088. https://doi.org/10.1038/s41558-023-01791-5

Casado, M., Landais, A., Picard, G., Arnaud, L., Dreossi, G., Stenni, B., & Prié, F. (2021). Water Isotopic Signature of Surface Snow Metamorphism in Antarctica. *Geophysical Research Letters*, *48*(17). https://doi.org/10.1029/2021GL093382

Casado, M., Landais, A., Picard, G., Münch, T., Laepple, T., Stenni, B., Dreossi, G., Ekaykin, A., Arnaud, L., Genthon, C., Touzeau, A., Masson-Delmotte, V., & Jouzel, J. (2018). Archival processes of the water stable isotope signal in East Antarctic ice cores. *The Cryosphere*, *12*(5), 1745–1766. https://doi.org/10.5194/tc-12-1745-2018

Casado, M., Münch, T., & Laepple, T. (2020). Climatic information archived in ice cores: Impact of intermittency and diffusion on the recorded isotopic signal in Antarctica. *Climate of the Past*, *16*(4), 1581–1598. https://doi.org/10.5194/cp-16-1581-2020

Chung, A., Parrenin, F., Mulvaney, R., Vittuari, L., Frezzotti, M., Zanutta, A., Lilien, D. A., Cavitte, M. G. P., & Eisen, O. (2025). *Age, thinning and spatial origin of the Beyond EPICA ice from a 2.5D ice flow model*. https://doi.org/10.5194/egusphere-2024-1650

Chung, A., Parrenin, F., Steinhage, D., Mulvaney, R., Martín, C., Cavitte, M. G. P., Lilien, D. A., Helm, V., Taylor, D., Gogineni, P., Ritz, C., Frezzotti, M., O'Neill, C., Miller, H., Dahl-Jensen, D., & Eisen, O. (2023). Stagnant ice and age modelling in the Dome C region, Antarctica. *The Cryosphere*, *17*(8), 3461–3483. https://doi.org/10.5194/tc-17-3461-2023

Craig, H., & Gordon, L. I. (1965). Deuterium and oxygen 18 variations in the ocean and marine atmosphere. *Laboratorio di geologia nucleare*.

Dallmayr, R., Goto-Azuma, K., Astrid Kjær, H., Azuma, N., Takata, M., Schüpbach, S., & Hirabayashi, M. (2016). A High-Resolution Continuous Flow Analysis System for Polar Ice Cores. *Bulletin of Glaciological Research*, *34*(0), 11–20. https://doi.org/10.5331/bgr.16R03

https://doi.org/10.5194/egusphere-2026-871
Preprint. Discussion started: 4 March 2026

582 Dallmayr, R., Meyer, H., Gkinis, V., Laepple, T., Behrens, M., Wilhelms, F., & Hörhold, M. (2025). Assessment
583 of continuous flow analysis (CFA) for high-precision profiles of water isotopes in snow cores. *The*
584 *Cryosphere*, *19*(3), 1067–1083. https://doi.org/10.5194/tc-19-1067-2025
585 Dansgaard, W. (1964). Stable isotopes in precipitation. *Tellus*, *16*(4), 436–468. https://doi.org/10.1111/j.2153-
586 3490.1964.tb00181.x
587 Dietrich, L. J., Steen-Larsen, H. C., Wahl, S., Jones, T. R., Town, M. S., & Werner, M. (2023). Snow-Atmosphere
588 Humidity Exchange at the Ice Sheet Surface Alters Annual Mean Climate Signals in Ice Core Records.
589 *Geophysical Research Letters*, *50*(20), e2023GL104249. https://doi.org/10.1029/2023GL104249
590 Dreossi, G., Masiol, M., Stenni, B., Zannoni, D., Scarchilli, C., Ciardini, V., Casado, M., Landais, A., Werner,
591 M., Cauquoin, A., Casasanta, G., Del Guasta, M., Posocco, V., & Barbante, C. (2024). A decade (2008–
592 2017) of water stable isotope composition of precipitation at Concordia Station, East Antarctica. *The*
593 *Cryosphere*, 18(9), 3911–3931. https://doi.org/10.5194/tc-18-3911-2024
594 Dutrievoz, N., Agosta, C., Risi, C., Vignon, É., Nguyen, S., Landais, A., Fourré, E., Leroy-Dos Santos, C.,
595 Casado, M., Masson-Delmotte, V., Jouzel, J., Dubos, T., Ollivier, I., Stenni, B., Dreossi, G., Masiol, M.,
596 Minster, B., & Prié, F. (2025). Antarctic Water Stable Isotopes in the Global Atmospheric Model LMDZ6:
597 From Climatology to Boundary Layer Processes. *Journal of Geophysical Research: Atmospheres*, *130*(5),
598 e2024JD042073. https://doi.org/10.1029/2024JD042073
599 Ekaykin, A. A., Lipenkov, V. Ya., Barkov, N. I., Petit, J. R., & Masson-Delmotte, V. (2002). Spatial and temporal
600 variability in isotope composition of recent snow in the vicinity of Vostok station, Antarctica: Implications
601 for ice-core record interpretation. *Annals of Glaciology*, *35*, 181–186.
602 https://doi.org/10.3189/172756402781816726
603 EPICA community members. (2004). Eight glacial cycles from an Antarctic ice core. *Nature*, *429*(6992), 623–
604 628. https://doi.org/10.1038/nature02599
605 Fisher, D. A., Reeh, N., & Clausen, H. B. (1985). Stratigraphic Noise in Time Series Derived from Ice Cores.
606 *Annals of Glaciology*, *7*, 76–83. https://doi.org/10.3189/S0260305500005942
607 Franzke, C. L. E., Barbosa, S., Blender, R., Fredriksen, H.-B., Laepple, T., Lambert, F., Nilsen, T., Rypdal, K.,
608 Rypdal, M., Scotto, Manuel G., Vannitsem, S., Watkins, N. W., Yang, L., & Yuan, N. (2020). The Structure
609 of Climate Variability Across Scales. *Reviews of Geophysics*, *58*(2), e2019RG000657.
610 https://doi.org/10.1029/2019RG000657

https://doi.org/10.5194/egusphere-2026-871
Preprint. Discussion started: 4 March 2026

Gautier, E., Savarino, J., Erbland, J., Lanciki, A., & Possenti, P. (2016). Variability of sulfate signal in ice core records based on five replicate cores. *Climate of the Past*, *12*(1), 103–113. https://doi.org/10.5194/cp-12-103-2016

Gautier, E., Savarino, J., Farquhar, J. (2018): 2600 years of stratospheric volcanism reconstruction through sulfate isotopes for Antarctic ice Dome C [dataset]. *PANGAEA*, https://doi.org/10.1594/PANGAEA.895169

Gautier, E., Savarino, J., Hoek, J., Erbland, J., Caillon, N., Hattori, S., Yoshida, N., Albalat, E., Albarede, F., & Farquhar, J. (2019). 2600-years of stratospheric volcanism through sulfate isotopes. Nature Communications, 10(1), 466. https://doi.org/10.1038/s41467-019-08357-0

Gautier, E., Savarino, J., Parrenin, F., Ritz, C., Possenti, P. (2021): Sulfate profile from 0 to 42 meters in a Little Dome C (Antarctica) ice core drilled in 2018 [dataset]. PANGAEA, https://doi.org/10.1594/PANGAEA.932490

Genthon, C., Six, D., Scarchilli, C., Ciardini, V., & Frezzotti, M. (2016). Meteorological and snow accumulation gradients across Dome C, East Antarctic plateau. *International Journal of Climatology*, *36*(1), 455–466. https://doi.org/10.1002/joc.4362

Gkinis, V., Simonsen, S. B., Buchardt, S. L., White, J. W., & Vinther, B. M. (2014). Water isotope diffusion rates from the NorthGRIP ice core for the last 16,000 years—Glaciological and paleoclimatic implications. *Earth and Planetary Science Letters*, *405*, 132–141. https://doi.org/10.1016/j.epsl.2014.08.022

Grimmer, M., Baggenstos, D., Schmitt, J., Krauss, F., Shackleton, S., Severinghaus, J. P., & Fischer, H. (2025). AMOC Modulates Ocean Heat Content During Deglaciations. Geophysical Research Letters, 52(6), e2024GL114415. https://doi.org/10.1029/2024GL114415

Groot Zwaaftink, C. D., Cagnati, A., Crepaz, A., Fierz, C., Macelloni, G., Valt, M., & Lehning, M. (2013). Event-driven deposition of snow on the Antarctic Plateau: Analyzing field measurements with SNOWPACK. *The Cryosphere*, *7*(1), 333–347. https://doi.org/10.5194/tc-7-333-2013

Herron, M. M., & Langway, C. C. (1980). Firn Densification: An Empirical Model. *Journal of Glaciology*, *25*(93), 373–385. https://doi.org/10.3189/S0022143000015239

Hersbach, H., Bell, B., Berrisford, P., Hirahara, S., Horányi, A., Muñoz-Sabater, J., Nicolas, J., Peubey, C., Radu, R., Schepers, D., Simmons, A., Soci, C., Abdalla, S., Abellan, X., Balsamo, G., Bechtold, P., Biavati, G., Bidlot, J., Bonavita, M., … Thépaut, J.-N. (2020). The ERA5 global reanalysis. *Quarterly Journal of the Royal Meteorological Society*, *146*(730), 1999–2049. https://doi.org/10.1002/qj.3803

https://doi.org/10.5194/egusphere-2026-871
Preprint. Discussion started: 4 March 2026

Hirsch, N., Zuhr, A., Münch, T., Hörhold, M., Freitag, J., Dallmayr, R., & Laepple, T. (2023). Stratigraphic noise and its potential drivers across the plateau of Dronning Maud Land, East Antarctica. *The Cryosphere*, *17*(10), 4207–4221. https://doi.org/10.5194/tc-17-4207-2023

Hourdin, F., Rio, C., Grandpeix, J.-Y., Madeleine, J.-B., Cheruy, F., Rochetin, N., Jam, A., Musat, I., Idelkadi, A., Fairhead, L., Foujols, M.-A., Mellul, L., Traore, A.-K., Dufresne, J.-L., Boucher, O., Lefebvre, M.-P., Millour, E., Vignon, E., Jouhaud, J., … Ghattas, J. (2020). LMDZ6A: The Atmospheric Component of the IPSL Climate Model With Improved and Better Tuned Physics. *Journal of Advances in Modeling Earth Systems*, *12*(7), e2019MS001892. https://doi.org/10.1029/2019MS001892

Huybers, P., & Curry, W. (2006). Links between annual, Milankovitch and continuum temperature variability. *Nature*, *441*(7091), 329–332. https://doi.org/10.1038/nature04745

Johnsen, S. J. (1977). *Stable isotope homogenization of polar- firn and ice*.

Johnsen, S. J., Clausen, H. B., Cuffey, K. M., Hoffmann, G., Schwander, J., & Creyts, T. (2000). Diffusion of stables isotopes in polar firn and ice: The isotope effect in firn diffusion. *Physics of Ice Core Records, Hokkaido University Press*, 121–140.

Jones, T. R., Cuffey, K. M., Roberts, W. H. G., Markle, B. R., Steig, E. J., Stevens, C. M., Valdes, P. J., Fudge, T. J., Sigl, M., Hughes, A. G., Morris, V., Vaughn, B. H., Garland, J., Vinther, B. M., Rozmiarek, K. S., Brashear, C. A., & White, J. W. C. (2023). Seasonal temperatures in West Antarctica during the Holocene. *Nature*, *613*(7943), 292–297. https://doi.org/10.1038/s41586-022-05411-8

Jouzel, J., & Masson-Delmotte, V. (2010). Paleoclimates: What do we learn from deep ice cores? *WIREs Climate Change*, *1*(5), 654–669. https://doi.org/10.1002/wcc.72

Jouzel, J., Masson-Delmotte, V., Cattani, O., Dreyfus, G., Falourd, S., Hoffmann, G., Minster, B., Nouet, J., Barnola, J. M., Chappellaz, J., Fischer, H., Gallet, J. C., Johnsen, S., Leuenberger, M., Loulergue, L., Luethi, D., Oerter, H., Parrenin, F., Raisbeck, G., … Wolff, E. W. (2007). Orbital and Millennial Antarctic Climate Variability over the Past 800,000 Years. *Science*, *317*(5839), 793–796. https://doi.org/10.1126/science.1141038

Kirchner, J. W. (2005). Aliasing in $1/f\,\alpha$ noise spectra: Origins, consequences, and remedies. *Physical Review E*, *71*(6), 066110. https://doi.org/10.1103/PhysRevE.71.066110

Küttel, M., Steig, E. J., Ding, Q., Monaghan, A. J., & Battisti, D. S. (2012). Seasonal climate information preserved in West Antarctic ice core water isotopes: Relationships to temperature, large-scale circulation, and sea ice. *Climate Dynamics*, *39*(7–8), 1841–1857. https://doi.org/10.1007/s00382-012-1460-7

https://doi.org/10.5194/egusphere-2026-871
Preprint. Discussion started: 4 March 2026

Laepple, T., Münch, T., Casado, M., Hoerhold, M., Landais, A., & Kipfstuhl, S. (2018). On the similarity and apparent cycles of isotopic variations in East Antarctic snow pits. *The Cryosphere*, *12*(1), 169–187. https://doi.org/10.5194/tc-12-169-2018

Landais, A., Casado, M., Prié, F., Magand, O., Arnaud, L., Ekaykin, A., Petit, J.-R., Picard, G., Fily, M., Minster, B., Touzeau, A., Goursaud, S., Masson-Delmotte, V., Jouzel, J., & Orsi, A. (2017). Surface studies of water isotopes in Antarctica for quantitative interpretation of deep ice core data. *Comptes Rendus. Géoscience*, *349*(4), 139–150. https://doi.org/10.1016/j.crte.2017.05.003

Libois, Q., Picard, G., Arnaud, L., Morin, S., & Brun, E. (2014). Modeling the impact of snow drift on the decameter-scale variability of snow properties on the Antarctic Plateau. *Journal of Geophysical Research: Atmospheres*, *119*(20), 11,662-11,681. https://doi.org/10.1002/2014JD022361

Lorius, C., Merlivat, L., & Hagemann, R. (1969). Variation in the mean deuterium content of precipitations in Antarctica. *Journal of Geophysical Research*, *74*(28), 7027–7031. https://doi.org/10.1029/JC074i028p07027

Lovejoy, S., & Schertzer, D. (2013). The Weather and Climate: Emergent Laws and Multifractal Cascades. In Cambridge University Press eBooks. https://doi.org/10.1017/cbo9781139093811

Masson-Delmotte, V., Delmotte, M., Morgan, V., Etheridge, D., Van Ommen, T., Tartarin, S., & Hoffmann, G. (2003). Recent southern Indian Ocean climate variability inferred from a Law Dome ice core: New insights for the interpretation of coastal Antarctic isotopic records. *Climate Dynamics*, *21*(2), 153–166. https://doi.org/10.1007/s00382-003-0321-9

Morgan, J. D., Buizert, C., Fudge, T. J., Kawamura, K., Severinghaus, J. P., & Trudinger, C. M. (2022). Gas isotope thermometry in the South Pole and Dome Fuji ice cores provides evidence for seasonal rectification of ice core gas records. *The Cryosphere*, *16*(7), 2947–2966. https://doi.org/10.5194/tc-16-2947-2022

Morgan, V. I. (1985). An oxygen isotope? Climate record from the Law Dome, Antarctica. *Climatic Change*, *7*(4), 415–426. https://doi.org/10.1007/BF00139056

Münch, T., Kipfstuhl, S., Freitag, J., Meyer, H., & Laepple, T. (2016). Regional climate signal vs. local noise: A two-dimensional view of water isotopes in Antarctic firn at Kohnen Station, Dronning Maud Land. *Climate of the Past*, *12*(7), 1565–1581. https://doi.org/10.5194/cp-12-1565-2016

Münch, T., Kipfstuhl, S., Freitag, J., Meyer, H., & Laepple, T. (2017). Constraints on post-depositional isotope modifications in East Antarctic firn from analysing temporal changes of isotope profiles. *The Cryosphere*, *11*(5), 2175–2188. https://doi.org/10.5194/tc-11-2175-2017

https://doi.org/10.5194/egusphere-2026-871
Preprint. Discussion started: 4 March 2026

Münch, T., & Laepple, T. (2018). What climate signal is contained in decadal- to centennial-scale isotope variations from Antarctic ice cores? *Climate of the Past*, *14*(12), 2053–2070. https://doi.org/10.5194/cp-14-2053-2018

Neumann, T. A., & Waddington, E. D. (2004). Effects of firn ventilation on isotopic exchange. *Journal of Glaciology*, *50*(169), 183–194. https://doi.org/10.3189/172756504781830150

Ollivier, I., Steen-Larsen, H. C., Stenni, B., Arnaud, L., Casado, M., Cauquoin, A., Dreossi, G., Genthon, C., Minster, B., Picard, G., Werner, M., & Landais, A. (2025). Surface processes and drivers of the snow water stable isotopic composition at Dome C, East Antarctica – a multi-dataset and modelling analysis. *The Cryosphere*, *19*(1), 173–200. https://doi.org/10.5194/tc-19-173-2025

Ollivier, I., Steen-Larsen, H. C., Dietrich, L. J., Cauquoin, A., Stenni, B., Werner, M., & Landais, A. (in review). Post-depositional Processes Alter the Seasonal and Multi-decadal Water Isotopic Records in Antarctic Snow and Firn. *Authorea Preprints*. DOI: 10.22541/au.175994561.12898624/v1

Persson, A., Langen, P. L., Ditlevsen, P., & Vinther, B. M. (2011). The influence of precipitation weighting on interannual variability of stable water isotopes in Greenland. *Journal of Geophysical Research*, *116*(D20), D20120. https://doi.org/10.1029/2010JD015517

Petteni, A., Fourré, E., Gautier, E., Spagnesi, A., Jacob, R., Akers, P. D., Zannoni, D., Gabrieli, J., Jossoud, O., Prié, F., Landais, A., Tcheng, T., Stenni, B., Savarino, J., Ginot, P., & Casado, M. (2025). Interlaboratory comparison of continuous flow analysis (CFA) systems for high-resolution water isotope measurements in ice cores. *Atmospheric Measurement Techniques*, *18*(20), 5435–5455. https://doi.org/10.5194/amt-18-5435-2025

Picard, G., Arnaud, L., Caneill, R., Lefebvre, E., & Lamare, M. (2019). Observation of the process of snow accumulation on the Antarctic Plateau by time lapse laser scanning. *The Cryosphere*, *13*(7), 1983–1999. https://doi.org/10.5194/tc-13-1983-2019

Pol, K., Masson-Delmotte, V., Johnsen, S., Bigler, M., Cattani, O., Durand, G., Falourd, S., Jouzel, J., Minster, B., Parrenin, F., Ritz, C., Steen-Larsen, H. C., & Stenni, B. (2010). New MIS 19 EPICA Dome C high resolution deuterium data: Hints for a problematic preservation of climate variability at sub-millennial scale in the "oldest ice". *Earth and Planetary Science Letters*, *298*(1–2), 95–103. https://doi.org/10.1016/j.epsl.2010.07.030

Risi, C., Bony, S., Vimeux, F., & Jouzel, J. (2010). Water-stable isotopes in the LMDZ4 general circulation model: Model evaluation for present-day and past climates and applications to climatic interpretations of

https://doi.org/10.5194/egusphere-2026-871
Preprint. Discussion started: 4 March 2026

tropical isotopic records. *Journal of Geophysical Research: Atmospheres*, *115*(D12), 2009JD013255. https://doi.org/10.1029/2009JD013255

Ritter, F., Steen-Larsen, H. C., Werner, M., Masson-Delmotte, V., Orsi, A., Behrens, M., Birnbaum, G., Freitag, J., Risi, C., & Kipfstuhl, S. (2016). Isotopic exchange on the diurnal scale between near-surface snow and lower atmospheric water vapor at Kohnen station, East Antarctica. *The Cryosphere*, *10*(4), 1647–1663. https://doi.org/10.5194/tc-10-1647-2016

Sime, L. C., Lang, N., Thomas, E. R., Benton, A. K., & Mulvaney, R. (2011). On high-resolution sampling of short ice cores: Dating and temperature information recovery from Antarctic Peninsula virtual cores. *Journal of Geophysical Research: Atmospheres*, *116*(D20). https://doi.org/10.1029/2011JD015894

Stenni, B., Scarchilli, C., Masson-Delmotte, V., Schlosser, E., Ciardini, V., Dreossi, G., Grigioni, P., Bonazza, M., Cagnati, A., Karlicek, D., Risi, C., Udisti, R., & Valt, M. (2016). Three-year monitoring of stable isotopes of precipitation at ConcordiaStation, East Antarctica. *The Cryosphere*, *10*(5), 2415–2428. https://doi.org/10.5194/tc-10-2415-2016

Stuart, R. H. (2024). Evolution of snow and air below the surface of the East Antarctic ice sheet (Doctoral dissertation, Université Paris-Saclay). https://theses.hal.science/tel-04996074v1

Touzeau, A., Landais, A., Morin, S., Arnaud, L., & Picard, G. (2018). Numerical experiments on vapor diffusion in polar snow and firn and its impact on isotopes using the multi-layer energy balance model Crocus in SURFEX v8.0. *Geoscientific Model Development*, *11*(6), 2393–2418. https://doi.org/10.5194/gmd-11-2393-2018

Touzeau, A., Landais, A., Stenni, B., Uemura, R., Fukui, K., Fujita, S., Guilbaud, S., Ekaykin, A., Casado, M., Barkan, E., Luz, B., Magand, O., Teste, G., Le Meur, E., Baroni, M., Savarino, J., Bourgeois, I., & Risi, C. (2016). Acquisition of isotopic composition for surface snow in East Antarctica and the links to climatic parameters. *The Cryosphere*, *10*(2), 837–852. https://doi.org/10.5194/tc-10-837-2016

Van Der Wel, L. G., Been, H. A., Van De Wal, R. S. W., Smeets, C. J. P. P., & Meijer, H. A. J. (2015). Constraints on the δ^2 H diffusion rate in firn from field measurements at Summit, Greenland. *The Cryosphere*, *9*(3), 1089–1103. https://doi.org/10.5194/tc-9-1089-2015

Vinther, B. M., Jones, P. D., Briffa, K. R., Clausen, H. B., Andersen, K. K., Dahl-Jensen, D., & Johnsen, S. J. (2010). Climatic signals in multiple highly resolved stable isotope records from Greenland. *Quaternary Science Reviews*, *29*(3–4), 522–538. https://doi.org/10.1016/j.quascirev.2009.11.002

https://doi.org/10.5194/egusphere-2026-871
Preprint. Discussion started: 4 March 2026

759 Wahl, S., Steen-Larsen, H. C., Hughes, A. G., Dietrich, L. J., Zuhr, A., Behrens, M., Faber, A. -K., & Hörhold,
760 M. (2022). Atmosphere-Snow Exchange Explains Surface Snow Isotope Variability. *Geophysical Research*
761 *Letters*, *49*(20). https://doi.org/10.1029/2022GL099529

https://doi.org/10.5194/egusphere-2026-871
Preprint. Discussion started: 4 March 2026

Appendix A

Table A1- Density profile of ICORDA-LDC firn core, measured on the field

Depth (m)	Density (g.cm-3)	Depth (m)	Density (g.cm-3)	Depth (m)	Density (g.cm-3)
1		41	0.629	81	0.774
2		42	0.631	82	0.776
3		43	0.633	83	0.783
4		44	0.666	84	0.810
5		45	0.649		
6		46	0.644		
7	0.388	47	0.649		
8	0.372	48	0.652		
9	0.385	49	0.667		
10	0.405	50	0.680		
11	0.420	51	0.681		
12	0.422	52	0.687		
13	0.442	53	0.681		
14	0.460	54	0.685		
15	0.497	55	0.683		
16	0.482	56	0.688		
17	0.487	57	0.687		
18		58	0.715		
19	0.504	59	0.695		
20	0.517	60	0.723		
21	0.529	61	0.705		
22	0.529	62	0.735		
23	0.535	63	0.725		
24	0.549	64	0.725		
25	0.544	65	0.730		
26	0.545	66	0.731		
27	0.557	67	0.724		
28	0.576	68	0.731		
29	0.570	69	0.742		
30	0.576	70	0.740		
31	0.576	71	0.757		
32	0.593	72	0.756		
33	0.585	73	0.763		
34	0.593	74	0.765		
35	0.597	75	0.772		
36	0.600	76	0.770		
37	0.607	77	0.762		
38	0.612	78	0.778		
39	0.608	79	0.793		
40	0.629	80	0.787		

https://doi.org/10.5194/egusphere-2026-871
Preprint. Discussion started: 4 March 2026

Appendix B

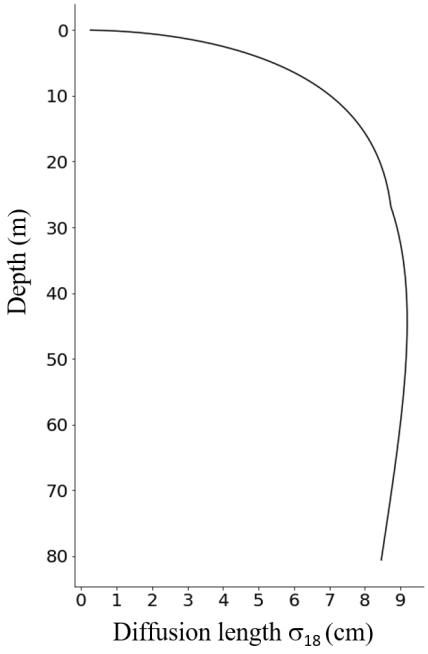

Figure B1 - $\delta^{18}O$ diffusion length at LDC following the classical isotopic diffusion scheme (Johnsen, 1977, Johnsen et al., 2000, Gkinis et al., 2014)

https://doi.org/10.5194/egusphere-2026-871
Preprint. Discussion started: 4 March 2026

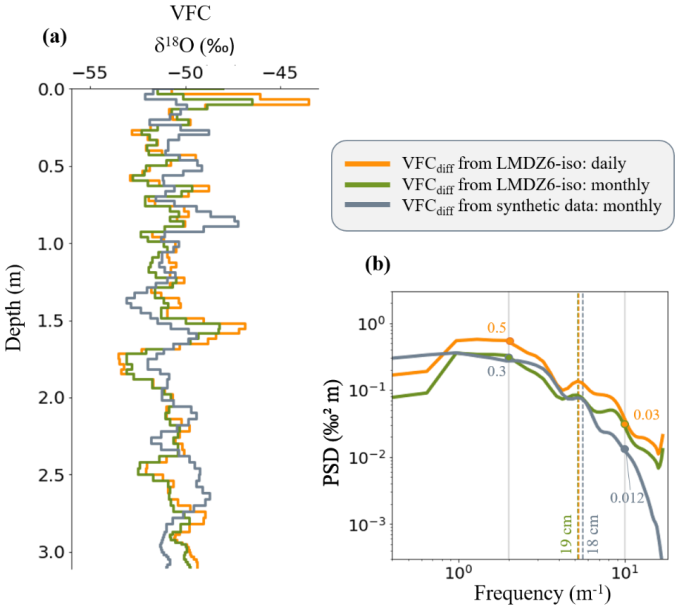

771

772 **Figure B2 - Comparison between $\delta^{18}O$ profiles and smoothed spectra of diffused VFC reconstructed from LMDZ6-iso**
773 **data in orange with daily data, in green with monthly data) and from monthly synthetic data (in dark grey) on the 3 m**
774 **top-scale (a). Profiles show similar variability with a slight shift in values, the VFC from LMDZ6-iso data is more**
775 **depleted by approximatively 2‰. The spectra (b) show the same characteristic peak at 18-19 cm, but a lowering of the**
776 **inflection point between daily and monthly LMDZ6-iso data. The spectral slope with monthly synthetic data is slightly**
777 **steeper than with monthly LMDZ6-iso data.**

778

https://doi.org/10.5194/egusphere-2026-871
Preprint. Discussion started: 4 March 2026

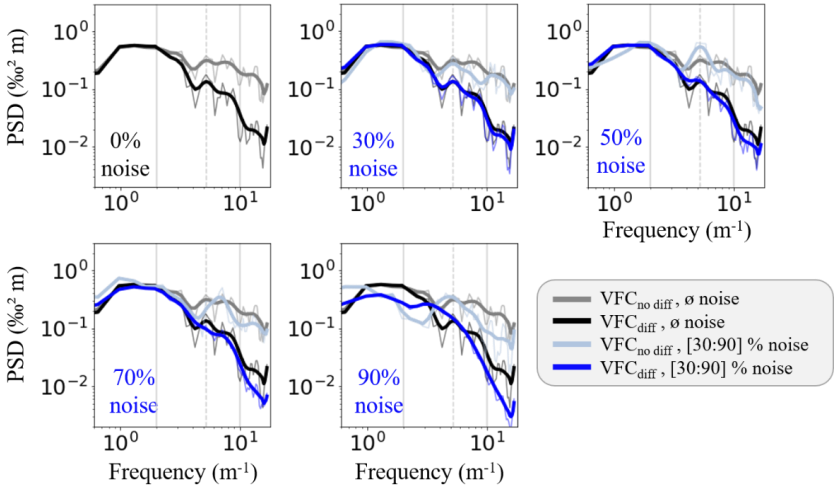

Figure B3 - Sensitivity tests of the impact of noise level on the VFC reconstruction on the 3 m top-scale, using LMDZ6-iso daily climatic data. We display the VFC spectra with noise from 0 to 90 % of noise, and without mixing. The raw VFC spectra (without noise) are displayed in grey (no diffusion) and black (with diffusion), while the noise tests are displayed in light blue (no diffusion) and dark blue (with diffusion). The light blue and dark blue thin lines correspond to the average spectra for ten emulations each, and the bold lines correspond to the smoothed spectra. The dashed line highlights the frequencies peak and the grey solid lines delimit the spectra slopes.

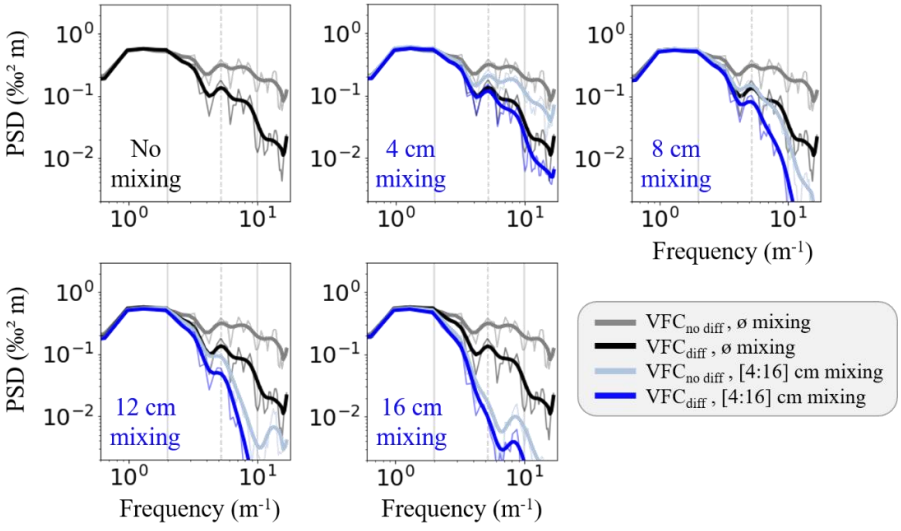

Figure B4 - Sensitivity tests of the impact of mixing scale on the VFC reconstruction on the 3 m top-scale, from LMDZ6-iso daily climatic data. We display the VFC spectra with mixing on scales from 0 to 16 cm, and without noise. The raw VFC spectra (without noise) are displayed in grey (no diffusion) and black (with diffusion), while the noise tests are displayed in light blue (no diffusion) and dark blue (with diffusion). The light blue and dark blue thin lines correspond to the average spectra for ten emulations each, and the bold lines correspond to the smoothed spectra. The dashed line highlights the frequencies peak and the grey solid lines delimit the spectra slopes.

https://doi.org/10.5194/egusphere-2026-871
Preprint. Discussion started: 4 March 2026

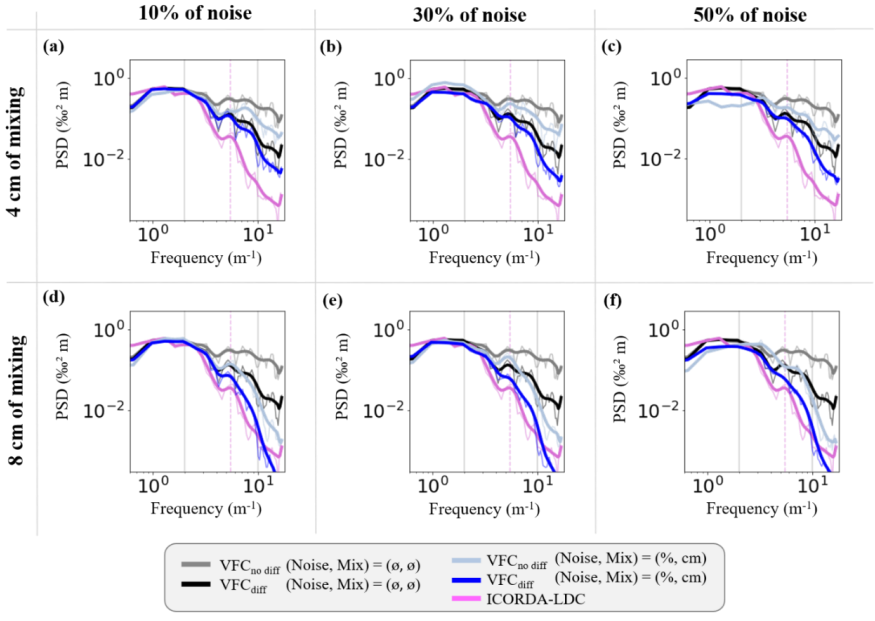

Figure B5 - Sensitivity tests to find the best fit between the VFC and ICORDA-LDC. Here we test a mixing scale of 4 cm with 0 %, 30 % and 50 % of noise (a, b, c), and a mixing scale of 8 cm with 0 %, 30 % and 50 % of noise (d, e, f). We chose these parameters in order to better fit the spectral slopes and to conserve the ICORDA-LDC frequency peak around 19 cm (dashed pink line). The light blue and dark blue thin lines correspond to the average spectra for ten emulations each, and the bold lines correspond to the smoothed spectra.

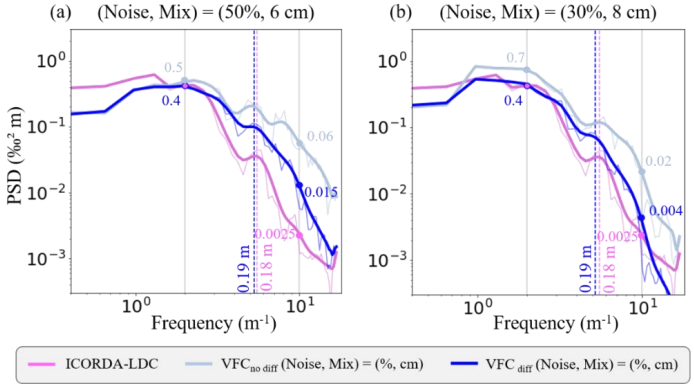

Figure B6 – VFC spectra on the 3 m top-scale, from LMDZ6-iso daily climatic data. VFC spectra comparison for best combinations of level of noise and mixing according to the RMS score, with (a) 50 % of noise and a 6 cm mixing layer, (b) 30 % of noise and an 8 cm mixing layer. The light blue and dark blue thin lines correspond to the average spectra for ten emulations each, and the bold lines correspond to the smoothed spectra.

https://doi.org/10.5194/egusphere-2026-871
Preprint. Discussion started: 4 March 2026

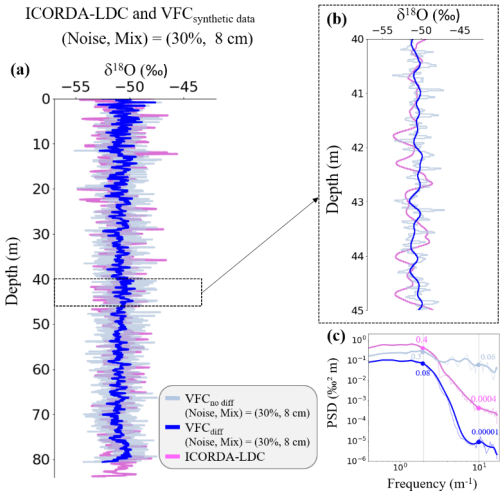

811

812 **Figure B7 - VFC $\delta^{18}O$ profile built from monthly synthetic climatic data, before (in light blue) and after (in dark blue)**
813 **diffusion, with 30 % noise and mixing on a 8-cm mixing scale (Noise, Mix) = (30 %, 8 cm), compared with ICORDA-**
814 **LDC $\delta^{18}O$ profile in pink (on the left) on the 80 m scale. On the right, we display the profile section between 40-45 m**
815 **depth and the signal spectra below. The light blue and dark blue thin lines correspond to the average spectra for ten**
816 **emulations each, and the bold lines correspond to the smoothed spectra.**

817

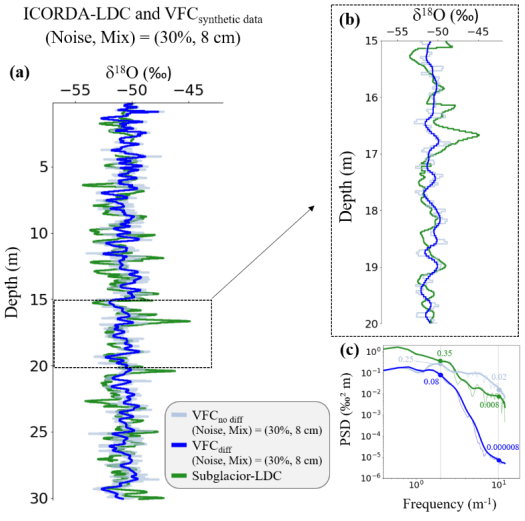

818

819

820 **Figure B8 - VFC $\delta^{18}O$ profile built from monthly synthetic climatic data, before (in light blue) and after (in dark blue)**
821 **diffusion, with 30 % noise and mixing on a 8-cm mixing scale (Noise, Mix) = (30 %, 8 cm), compared with Subglacior-**
822 **LDC $\delta^{18}O$ profile in green (on the left) on the 80 m scale. On the right, we display the profile section between 15-20 m**
823 **depth and the signal spectra below. The light blue and dark blue thin lines correspond to the average spectra for ten**
824 **emulations each, and the bold lines correspond to the smoothed spectra.**